The influence of hydrogen on cyclic plasticity of oriented nickel single crystal. Part II: Stability of edge dislocation dipoles

G. Hachet, A. Metsue, A. Oudriss, X. Feaugas

Version of Record: https://www.sciencedirect.com/science/article/pii/S0749641919306400
Manuscript_128eddd008c10b91fe30ee123d824478

The influence of hydrogen on cyclic plasticity of <001> oriented nickel single crystal. Part II: Stability of edge dislocation dipoles

G.Hachet(*), A.Metsue, A.Oudriss and X.Feaugas

La Rochelle University, LaSIE UMR CNRS 7356, Avenue Michel Crépeau, 17000 La Rochelle, France.
(*)Corresponding author: guillaume.hachet@gmx.com

Abstract: A competition between hardening and softening hydrogen effects on the cyclic behaviour of <001> oriented nickel single crystal have been observed and discussed in terms of effective and back stresses partitioning, but also in terms of composite model which illustrates the interaction between hydrogen and dislocation organisation. The hydrogen hardening associated with dislocation wall phase is a key feature which has been discussed and elucidated at edge dislocation dipoles scale using atomic calculations in nickel single crystal. The aim of our study was to evaluate the stability of this dislocation organisation in the presence of hydrogen, vacancies and vacancy clusters. As the main result, we noted that hydrogen in Cottrell's atmosphere hardens dipole configurations following solid solution strengthening and vacancies induced by hydrogen incorporation and cyclic loading attenuate this result. Moreover, the consequences of vacancies are more important when they are regrouped as clusters than when they are homogeneously distributed in the Cottrell's atmosphere. Such results can explain the complex behaviour of the wall phase and the consequence on long-range internal stresses observed in the first part of this study.

Keywords: A: edge dislocation dipole, A: fatigue; B: crystal plasticity, C: numerical algorithms; hydrogen

1. Introduction

Hydrogen-dislocation interactions and their impact on the plasticity are well accepted as key features in understanding hydrogen embrittlement (Delafosse, 2012; Feaugas and Delafosse, 2019; Lynch, 2019; Robertson et al., 2015, 2009). The effect of hydrogen on the mechanical behaviour at multi-scale of metallic materials under tensile loading has been widely studied (Castelluccio et al., 2018; Delafosse, 2012; Feaugas and Delafosse, 2019; Robertson et al., 2015) but under cyclic loading the consequences of hydrogen has been less investigated (Magnin et al., 2001). Therefore, we purpose this multi-scale analysis to capture the fundamental phenomenon occurring under cyclically strained FCC metal-containing hydrogen.

This multi-scale study is composed of two articles (part I: (Hachet et al., 2019) and part II: this work) and aims to determine the consequences of hydrogen on the mechanical response of cyclically strained nickel single crystal oriented for multi-slips (load axis parallel to <001>). The first article, based on a multi-scale experimental analyses, highlights a softening effect of hydrogen when the metal was cyclically strained at hardening stage II_0 and III_0, and a minor hardening was noted at stage III. The hardening and softening effects have been discussed in terms of effective and back stresses partitioning to track respectively the impact of hydrogen on the short and long-range interactions of dislocations. The softening effect has been attributed to a reduction of the effective stress τ_{eff} and suggests an elastic shielding of the solute, which is in relation with the HELP model (Hydrogen-Enhanced Localized Plasticity) (Beachem, 1972; Birnbaum and Sofronis, 1994; Delafosse, 2012; Delafosse and Magnin, 2001; Hachet, 2018). A more complex behaviour has been observed for the back stress τ_X and will be investigated in the present article using atomic calculations. Moreover, cyclic tests induced specific dislocation organisations, visible at lower length

scales, similar to a composite organisation composed of dipolar wall and channel phases, in agreement with the literature (Argon, 1996; Laird, 1996; Li et al., 2011; Mughrabi, 1988, 1987, 1983). From the transmission electron microscopy (TEM) characterisation and nano-indentation (NI) tests, we have noted that hydrogen hardens wall phase while softens the channel phase for all plastic strain amplitudes studied (Hachet et al., 2019).

Since two phases have been induced by fatigue, different mechanisms occurred in each phase and hydrogen impacts differently these phases. In the channel phase, it has been well established that cross-slip events of screw dislocations occurred (Bonneville and Escaig, 1979; Escaig, 1968; Hull and Bacon, 2011; Rao et al., 2010; Saada, 1991). The energy activation of this mechanism has been characterised by molecular dynamics (MD) simulations in nickel single crystal (Rao et al., 2011, 2010). The authors have noted in the presence of forest dislocations, the activation energy decreased and the probability of cross-slip event increased. Moreover, this energy depends on the dissociation distance of partial dislocations in FCC crystals since screw dislocations are dissociated in these materials. Therefore, previous studies have been devoted to determine the most favourable segregation sites of hydrogen in dissociated screw dislocations in nickel (Tang and El-Awady, 2012). The authors have highlighted that the binding energy is low enough for hydrogen to segregate into the stacking fault ribbon in case of dissociated screw dislocation only. Moreover, another study has investigated the effect of hydrogen incorporated into the stacking fault ribbon on the probability of cross-slip event to occur (Wen et al., 2007). The latter study indicates that the solute increases the dissociation distance between partial dislocations and induced an increase of 55% of the cross-slip activation energy. Experimentally, when hydrogen is pre-charged in nickel single crystal cyclically strained and oriented for single slip (Magnin et al., 2001) or multi-slips (Hachet et al., 2019), it has been demonstrated that the solute delays the beginning of the hardening stage III_0. This result is a direct observation of the reduction of cross-slip events due to hydrogen incorporation (Delafosse and Magnin, 2001; Magnin et al., 2001). Therefore, in channel phase, hydrogen increases the mobility of dislocations locally, which induces a localisation of plasticity, according to the proposed HELP model, but also delays the cross-slip events of screw dislocations. This induce a softening of the channel phase and reduced the effective stress noted in the first part of this study.

As for the complex behaviour of the back stress observed when hydrogen is pre-charged in cyclically strained nickel single crystal, it is related to the hardening of the wall phase due to the hydrogen incorporation. It is well-known that cyclic loadings induced a dipolar configuration of edge dislocations into the wall phase (Li et al., 2011; Mughrabi, 1983; Tippelt et al., 1997) and the strength of the phase depends on the elastic equilibrium of the edge dislocation dipole (Antonopoulos et al. 1976; Tichy and Essmann, 1989). Different dipole mechanism formations have been proposed (Fourie and Murphy, 1962; Kroupa, 1966; Price, 1961; Segall et al., 1961; Tetelman, 1962) and have been revisited in a more recent study assisted by computational simulations (Erel et al., 2017; Veyssière and Chiu, 2007). Asides from mechanisms related to climb processes of dislocations, edge dislocation dipoles are mostly formed in channel phase, then, it is assumed they are quickly pushed back in the wall phase and agglomerated in this phase. Extensive work has been performed in literature to describe the interaction between hydrogen and edge dislocations (Chateau et al., 2002; Girardin and Delafosse, 2004; Gu and El-Awady, 2018; Sofronis and Birnbaum, 1995; Tang and El-Awady, 2012; Tehranchi et al., 2017; von Pezold et al., 2011). In case of FCC crystal, the solute segregated mainly into the tensile area of dislocations (Cottrell, 1953; Hirth and Lothe, 1982; Kirchheim, 1981; Sofronis and Birnbaum, 1995) to the point that some work suggests that nano-sized hydrides can be formed in this area (von Pezold et al., 2011). Such behaviour induces a reduction of the stacking fault ribbon and amplify the shielding effect of hydrogen described by HELP mechanisms (von Pezold et al., 2011).

However, it is also well-known that hydrogen and fatigue loadings favour the formation of vacancies and vacancy clusters (Carr and McLellan, 2004; Essmann and Mughrabi, 1979; Fukai, 2005; Harada et al., 2005; Nagumo, 2016; Oudriss et al., 2012; Polak, 1969; Saada, 1960; Saada and Veyssière, 2002). Vacancies, unlike hydrogen atoms, are formed in the compressive area of edge dislocations in FCC metals when they are in the vicinity of these defects (Clouet, 2006; Sato et al., 2004). Therefore, in the case of vacancies induced by the hydrogen incorporation close to edge dislocations, the study becomes more complicated. Since both dislocations and vacancies have a trapping effect on hydrogen, previous studies have been performed with atomic calculations (Bhatia et al., 2014; Li et al., 2015; Tehranchi et al., 2017; Zhu et al., 2017). Notably, it has been pointed out that vacancies and hydrogenated vacancies can reduce or increase the yield stress of the material, inducing softening or hardening mechanisms (Tehranchi et al., 2017). In the latter study, the impact of such defects has been discussed with solid solution strengthening theory in order to establish the connection between the strength, solute concentration, and misfit strain tensor. The formation of vacancies also occurred when FCC metals are cyclically strained, mostly due to the annihilation of dislocations and non-conservative movement of jogged dislocations (Essmann and Mughrabi, 1979; Man et al., 2009; Saada, 1960). Thus, two sources of vacancy formations around dislocations dipole are noted for cyclically strained nickel-hydrogen systems.

The effect of the same solute on the strength of solids can be opposite depending on its concentration, the particle size or ageing time (Hull and Bacon, 2011). Therefore, solid solution strengthening theory has been developed in order to describe the experimental effect of solute (Cahn and Haasen, 1996; Fleischer, 1963; Friedel, 1964; Kubin, 1993; Labusch, 1970) and has been used to describe effect of impurities on dislocations with atomic calculations (Patinet and Proville, 2008; Tehranchi et al., 2017; Varvenne et al., 2017; Zhao et al., 2018). In the case of vacancies and hydrogenated vacancies interactions with edge dislocations, Tehranchi *et al.* have found with numerical methods that vacancies harden edge dislocations and hydrogenated vacancies attenuate this results (Tehranchi et al., 2017). However, questions remaining the effect of hydrogen alone and vacancies induced by hydrogen incorporation on edge dipolar configurations are still unknown and will be investigated in this work, since this dislocation organisation corresponds more exactly to the walls observed when the metal is cyclically strained. Since the softening of channel phase is easily explained from the HELP model, this work focuses mainly on the interactions between hydrogen and the fatigue-induced defects using a numerical approach in order to understand the hardening of the wall phase due to hydrogen incorporation and its interaction with edge dislocation dipoles.

In this article, we first detail the numerical approach to evaluate the stability of edge dislocation dipoles in the presence of hydrogen atoms and vacancies, since the strength of the dipolar wall phase developed during cyclic loading depends on the elastic equilibrium of the dipolar configuration. In parallel to these calculations, we have developed an analytical approach based on the elastic theory and solid solution strengthening of dislocations. The results are compared and discussed in the followings. From these approaches, a competition of the effect of hydrogen and vacancies has been noted and compared with the results from the first part of this study in order to explain the hardening of the wall phase and the complex behaviour of the back stress.

2. Computational details and theory

2.1 Interatomic potentials and edge dislocation dipoles formation

To describe the behaviour of hydrogen atoms into nickel matrix with MD simulations, the EAM (embedded atoms model) potential of Angelo *et al.* (Angelo et al., 1995) is widely used in the literature (Hallil et al., 2018; Tang and El-Awady, 2012; Tehranchi et al., 2017; Tehranchi and Curtin,

2017; von Pezold et al., 2011; Wen et al., 2007; Xu et al., 2002; Zhao et al., 2018; Zhou et al., 2016, 2018). Therefore, we have first compared this potential with a MEAM (modified EAM) potential which takes into account the angular forces of atoms. It has been developed by Lee *et al.* and Ko *et al.* and aims to describe hydrogen atoms in nickel matrix (Ko et al., 2011; Lee et al., 2003). The comparison between both potentials has been done on the stability of edge dislocations dipoles of pure nickel, before the incorporation of the solute or the formation of vacancies.

In this work, large-scale MD simulations have been performed using LAMMPS code (Plimpton, 1995) and we have used OVITO (Stukowski, 2010) to visualise the relaxed atomic structures. For all calculations, the X, Y and Z axes have been respectively parallel to $[1\bar{1}0]$, $[111]$ and $[\bar{1}\bar{1}2]$ directions in order to investigate the stability of edge dislocation dipoles of nickel in the presence of hydrogen and vacancies. Moreover, the use of periodic boundary condition implies each dipole can interact with an infinite number of dislocations. Therefore, two dipole configurations, which are called multipole and isolated dipole configurations have been studied. For both cases, the formation of dipolar configuration has been performed following the method presented in the work of Tichy *et al.* (Tichy and Essmann, 1989) and Chang *et al.* (Chang et al., 2002). The dislocation dipole with a height of N times the $\{111\}$ interplanar distance d_{111} ($d_{111} = a\sqrt{3}/3$ and a the lattice parameter of the metal) has been introduced by removing two atomic columns with a dimension of $1/2\,[1\bar{1}0] \times h$ with h the dipole height equal to $N \times d_{111}$.

For the multipole configuration, dislocations have been placed at a height h which varies from 1.2 nm to 61 nm and the box standards along the X and Y axis have been equal to $2h$. Hence, the periodic boundary condition implies that the image dislocations, which are at the same distance of the ones into the simulation cell and induced a multipole structure. The lattice repetition along the Z axis has been fixed to two for all simulations and the number of atoms was between 456 and 1174800 nickel atoms (depending on the dipole height). The isolated dipole configuration consists in representing the behaviour of isolated edge dislocation dipoles. Therefore, the box standards along X and Y axes have been fixed at 100 nm and the dipole height has stayed between 0.6 nm and 50 nm before the energy minimisation of each simulation cells at 0K. For this configuration, we assumed the interactions with the dislocation images are negligible since the height h is low in comparison with the box standards along X and Y. The box standard along Z axis has been also fixed to two, thus the number of nickel atoms has been varying between 751440 and 752632 atoms depending on the dipole height.

The energy minimisation of each simulation cells has been first performed at constant volume, then with an applied pressure equal to 0 GPa at the boundaries of the simulation cell using a conjugate gradient algorithm for both configurations. Here, each dislocation has been dissociated into two partial dislocations separated by a stacking fault represented by red and blue atoms in **figure 1(a)**. After the energy minimisations of the simulation cells, the dissociation distance d_{disso} between two partial dislocations and the deviation angle φ between both dislocations (illustrated in **figure 1.(b)**) have been calculated as a function of the dipole height h. These calculations have been performed in order to evaluate the most suited potential and best dipole configurations in pure nickel to incorporate hydrogen and to form vacancies.

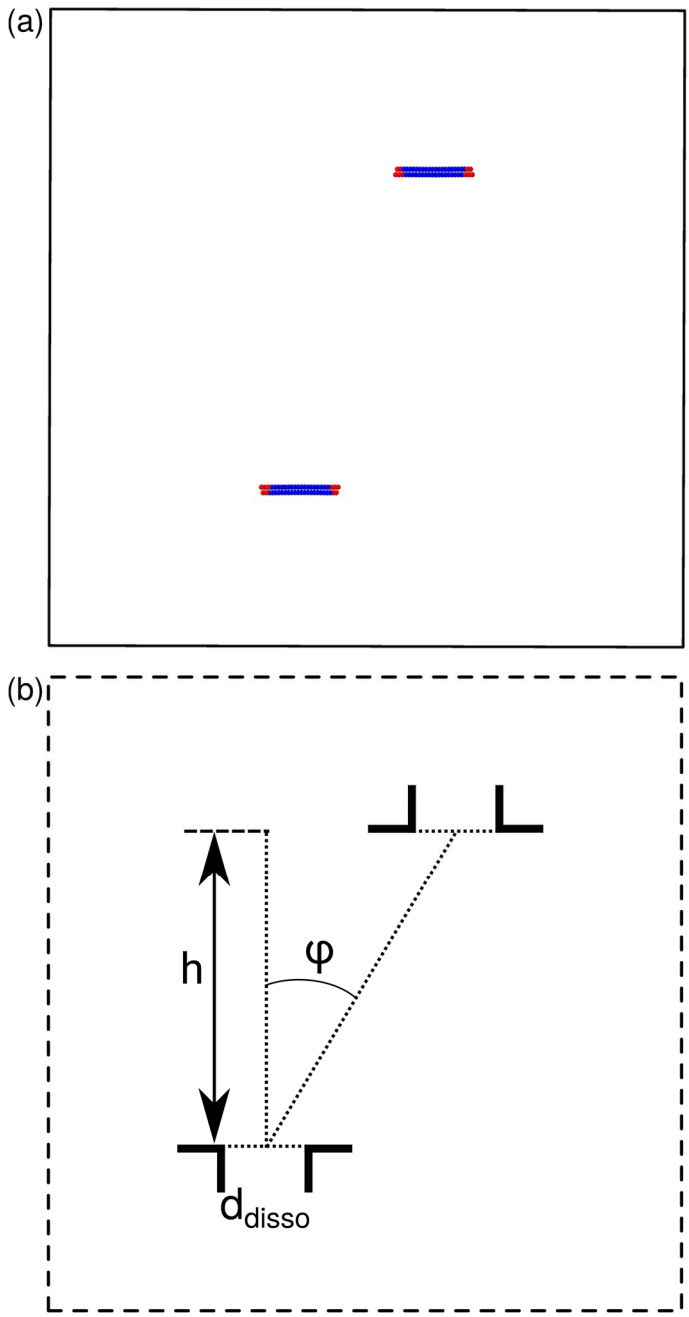

Figure 1: Relaxed simulation cell containing 2 edge dislocations (a). For clarity, only atoms belonging to the dislocation are shown and their colours are chosen from the common neighbour analysis. Hence, the blue atoms represent the stacking fault while the red ones are the core of the partial dislocations. Sketch of the simulation cell after the energy minimisation highlighting the dissociation distance d_{disso} and the deviation angle φ between both dislocations (b).

2.2 Hydrogen incorporation and vacancies formation

Hydrogen atoms have been incorporated into simulation cells containing edge dislocation dipoles in order to evaluate their consequences. To incorporate hydrogen atoms, the stress tensor of each nickel atom has been firstly calculated after the formation of the dislocation dipoles. The hydrostatic pressure acting on each atom has been evaluated and the solute has been incorporated in the tensile area of each dislocation since hydrogen segregates more favourably into this area around edge dislocations (Cottrell, 1953; Hirth and Lothe, 1982; Kirchheim, 1981; Sofronis and Birnbaum,

1995). For the sake of clarity, we have chosen to limit the dynamic interaction between the cloud of impurities (*i.e.*: Cottrell's atmosphere) and the dislocation when the hydrostatic pressure P was larger or equal to 10 GPa instead of adjusting gradient of hydrogen concentration around the dislocation. This method was used in order to simply quantify the local concentration of hydrogen. Then, 25 and 50 hydrogen atoms have been randomly incorporated per lattice repetition along the Z axis into the simulation cell. Because the lattice repetition along the Z axis has been increased to 16, 400 and 800 solute atoms have been incorporated in each cell.

The energy minimisation has been performed by imposing a pressure equal to 0 GPa at the limits of the simulation cell after the incorporation of hydrogen. The latter segregates to its closest interstitial sites during this step. Then, each simulation cell has been relaxed at 100K at constant volume during 200 ns allowing hydrogen atoms to segregate from a tetrahedral site to an octahedral site since the last is the most favourable interstitial site for hydrogen incorporation (Connétable et al., 2014; Metsue et al., 2016; Nazarov et al., 2014). Finally, the last energy minimisation has been performed at 0K before evaluating the stability of edge dislocation dipoles in the presence of hydrogen.

The stability of edge dislocation dipoles has been also performed in the presence of vacancies besides hydrogen. In previous work, notably related to the irradiated materials, it has been well established that vacancies are formed in the compressive area of edge dislocations in FCC metals (Clouet, 2006; Sato et al., 2004). When nickel-hydrogen systems is cyclically strained, two sources of vacancy formation are obtained. In this situation, the interaction between hydrogen and vacancy does not exactly corresponds to hydrogenated vacancy and these point defects around dislocations can segregate to positions where they are not stable without hydrogen. For instance, **supplementary material 1** presents an example of relaxed (at 100K for 200 ns) dislocation dipoles configurations with vacancies in the tensile areas of edge dislocations (similar to a dipolar configuration with vacancies when hydrogen is desorbed). In this case, the thermal relaxation allows the dislocation to move in its glide plane. Thus, when vacancies have been formed by the solute and the latter is desorbed, edge dislocation dipoles will not trap the point defect. Therefore, the study has been focused on the effect of formed vacancies and clusters in the presence of hydrogen on the stability of edge dislocation dipoles. Moreover, we have evaluated in previous studies that the concentration of vacancies is in the same order of the concentration of hydrogen when it is incorporated into nickel single crystal (Hachet et al., 2018). Therefore, we have chosen to randomly form 25 vacancies per lattice repetition along the Z axis into simulation cells containing hydrogen. Since there are 16 lattice repetitions along this axis, 400 (200 per Cottrell's atmosphere) vacancies have been incorporated. These points defects have been formed before the relaxation at 100K of the simulation cells.

Finally, since it has been observed with TEM images that pre-charged hydrogen-induced vacancy clusters about 2 nm of diameter (Hachet et al., 2018), we have studied the stability of edge dislocation dipoles with vacancy clusters besides hydrogen. Such atomic calculations are performed in order to compare the effect of homogeneously distributed vacancies to the same amount of vacancies but regrouped at one area in the Cottrell's atmosphere. Hence, we have formed an isotropic sphere of vacancies about 0.8 nm (which correspond to approximately 200 vacancies) in each Cottrell's atmosphere of the different simulation cells containing hydrogen atoms.

2.3 Stability of dislocation dipoles from elastic theory and solid solutions strengthening theory

The stability of edge dislocation dipoles in pure nickel has also been calculated from elastic theory for isolated dipole and multipole configurations by determining the critical passing stress τ_P needed to break the elastic equilibrium of the configuration. In case of isolated configuration, details

can be found in various work (Cai and Nix, 2016; Friedel, 1964; Hirth and Lothe, 1982; Kroupa, 1966; Veyssière and Chiu, 2007; Wang et al., 2008). Assuming two dislocations are in a configuration identical as the one presented in **figure 2(a)**, dislocation 1 is fixed and the temperature of the system is low enough to neglect the climb force, the stress fields around dislocation 2 is:

$$\tau_{xy}^{iso} = \frac{\mu b}{2\pi(1-\nu)h}\frac{\beta(\beta^2-1^2)}{(\beta^2+1^2)^2} \quad (1)$$

Where $\beta = x/h$, the shear modulus $\mu = \mu\{111\}\langle 110\rangle$ and the Poisson ratio $\nu = \nu\{111\}\langle 100\rangle$ are equal to 74 GPa and 0.23 (values calculated from the elastic constants determined by DFT calculations in previous work (Hachet et al., 2018)). Without any external force, the dipolar configuration is in elastic equilibrium when $\beta = 0$ and $\beta = 1$ (or when the deviation angle $\varphi = arctan(\beta)$ is equal to 0° or 45°). Moreover, when the system is sheared, the critical passing stress τ_P needed to break the elastic equilibrium can be determined from equation (1) and is equal to (the development is presented in **supplementary material 2**):

$$\tau_P^{iso} = 0.125\frac{\mu b}{\pi(1-\nu)h} \quad (2)$$

This result stands for undissociated isolated dislocation dipoles, but the atomic simulations present dissociated dislocations. Since it has been noted in previous work that the dissociation has a minor effect of the stability of edge dislocation dipole (Veyssière and Chiu, 2007), we assume that dissociated dislocations have an elastic behaviour similar to undissociated dislocations in the following the analytical approach of this study.

In case of multipole configuration, we have assumed the elastic stress fields induced by dislocations placed at a distance larger than $2h$ are negligible in comparison with elastic stress fields induced by the closest dislocations. A representation of the configuration is displayed in **figure 2.b**. In this analytical approach, we have supposed that dislocation 2 is fixed, in addition to its dislocation images 3, 4 and 5, inducing a stress field around dislocation 1 equal to:

$$\tau_{xy}^{multi} = \frac{\mu b}{\pi(1-\nu)h}\left[\frac{\beta(\beta^2-1)}{(\beta^2+1)^2} - \frac{(2-\beta)((2-\beta)^2-1)}{((2-\beta)^2+1)^2}\right] \quad (3)$$

Unlike isolated edge dislocation dipoles, τ_{xy}^{multi} of equation (3) is not equal to 0 when $\beta = 0$ in case of multipole configuration. Assuming only the 4 nearest dislocation neighbours impact a dislocation, the configuration is in elastic equilibrium when $\beta \simeq 0.425$ and $\beta = 1$ (or when the deviation angle φ is about 23° or 45°). Then, following the method presented in **supplementary materials 2**, the critical passing stress for multipole configurations τ_P^{multi} has been obtained analytically and is about:

$$\tau_P^{multi} \simeq 0.419\frac{\mu b}{\pi(1-\nu)h} \quad (4)$$

Hence, the strength of edge dislocation dipole has been expressed analytically with equations (2) and (4) as a function of the dipole height. These equations have been compared with the atomic

simulations of nickel single crystal containing edge dislocation dipoles since unrealistic strain rate has to be applied to shear the simulation cell (Wang et al., 2008).

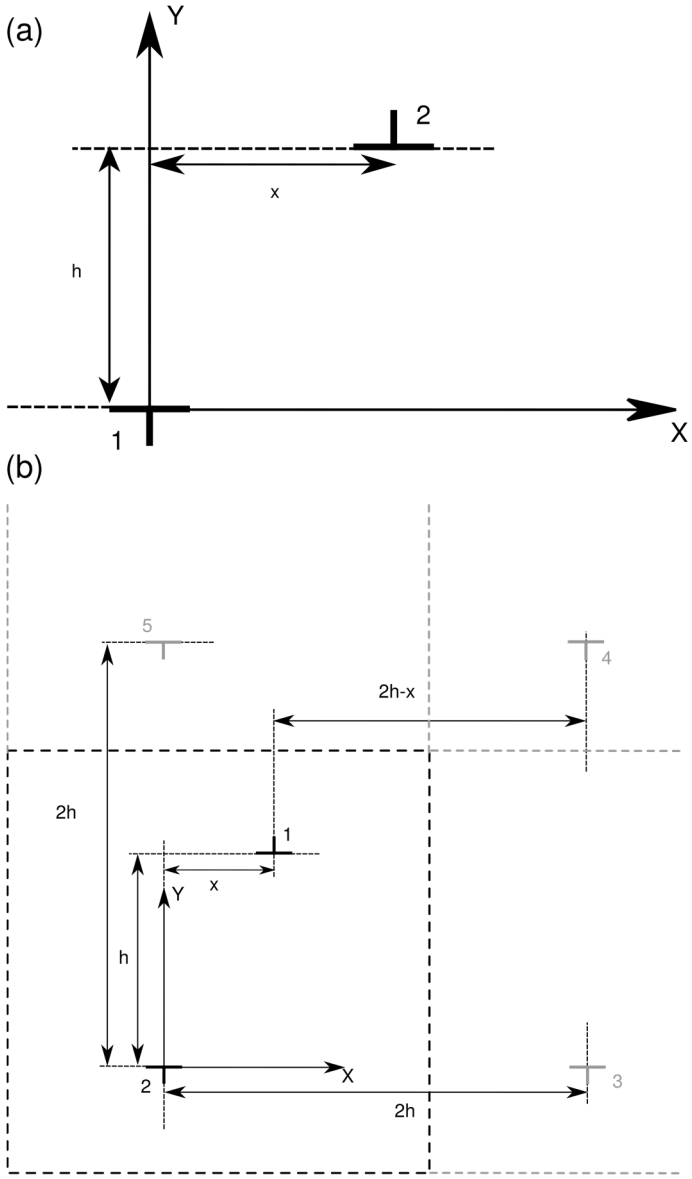

Figure 2: Isolated edge dislocation dipole configuration (Kroupa, 1966) (a). Sketch of edge dislocation multipole configuration, the grey dislocations represents the images of dislocation 2 (b).

Moreover, to observe the impact of hydrogen and vacancies on those dislocation organisations, models based on solid solution strengthening theory have been used in this work. They have been proposed in the literature to describe the interaction between impurities and mobile dislocations as a function of the different dispersive states of the point defects (Fleischer, 1963; Friedel, 1964; Kubin, 1993; Labusch, 1970). This dispersive state is represented with a dimensionless parameter η_0 (Cahn and Haasen, 1996; Labusch, 1970):

$$\eta_0 = \frac{w}{b}\left(\frac{2c_H\Gamma_L}{f_{max}}\right) \tag{5}$$

With w representing the interaction distance of the solute with the dislocation, which is often evaluated between 2 and 3 times the Burgers' vector (Kubin, 1993) and therefore, is about 2.5b in this study. f_{max} is the maximum interaction force between solutes and dislocation, which depends on a mean pinning coefficient $\bar{\alpha}$ (Kubin, 1993; Patinet and Proville, 2008) and Γ_L the line tension of edge dislocations, which is calculated from the classical estimation, *i.e.*: $E_L = \mu\, b^2/2$. The dislocation in our calculations are dissociated, therefore the stacking fault needs to be taken into account, hence $E_{\mathrm{Le}} = 0.95E_L$ (Patinet and Proville, 2008). Finally, we applied a well-known result from the isotropic elastic theory in order to determine the line tension (Hirth and Lothe, 1982; Patinet and Proville, 2008):$\Gamma_{\mathrm{L}} = E_{\mathrm{Le}}(1-2\nu)$. When $\eta_0 << 1$, the observed hardening is due to dilute, strong obstacles interacting with the dislocation. In this case, the classical model of Friedel-Fleischer (FF) adequately represents the hardening of the material due to the solute and is written (Fleischer, 1963; Friedel, 1964):

$$\Delta\tau^{FF} = \frac{f_{max}}{b^2}\left(\frac{c_H}{2\Gamma_L}\right) \tag{6}$$

However, when $\eta_0 > 1$, the hardening is due to a more concentred, weak obstacles interacting with the dislocation. The Mott-Nabarro-Labusch model is more adequate to describe the observed hardening and it is written (Cahn and Haasen, 1996; Labusch, 1970):

$$\Delta\tau^{MNL} = \Delta\tau^{FF}(1+2.5\eta_0)^{(1/3)} \tag{7}$$

This set of equations has been used in the followings to question the data obtained by atomic calculations.

3. Results

The aims of this study is to investigate why hydrogen hardens the wall phase and to understand the consequence on the back stress obtained in the first part of the study. Therefore, we have evaluated the stability of edge dislocation dipoles of nickel single crystal in the presence of hydrogen and vacancies. However, we first have performed atomic calculations on edge dislocation dipoles on pure nickel with two different potentials which can describe nickel and hydrogen atoms (Angelo et al., 1995; Ko et al., 2011; Lee et al., 2003). A comparison of calculations performed with both potentials is firstly presented for pure nickel. Then, we have incorporated hydrogen atoms into simulation cells containing edge dislocation dipoles. After a careful relaxation of the simulation cells, the lasts have been sheared in order to evaluate the critical passing stress τ_P and this critical stress has been compared with the analytical approach presented in the previous section of this manuscript. Finally, we have also sheared simulation cells containing vacancies and vacancy clusters besides hydrogen in order to evaluate their impact of the stability of edge dislocation dipoles.

3.1 Relaxed dipole configurations at 0K

First, atomic calculations with EAM and MEAM potentials have been conducted on edge dislocation dipoles of pure nickel. We have compared both potentials in order to use the most suited one to study the consequences of hydrogen on the stability of edge dislocation dipoles. The dissociation distance d_{disso} and the deviation angle φ have been determined from the energy of each atom into the simulation cell after the energy minimisation (detailed in **section 2.1**). The dissociation distance has been defined as the distance between the two nickel atoms which have their highest potential energy in the slip plane of each dislocation and the deviation angle has been defined as the angle between the middle of the stacking fault ribbons of each dislocation. Both quantities have been represented in **figure 3** for multipole and isolated dipole configurations with EAM and MEAM potentials as a function of the dipole height h.

Calculations conducted with EAM potential present a larger dissociation distance for all dipole height and both configurations. We noted d_{disso}^{EAM} ~3 nm and d_{disso}^{MEAM} ~2 nm, both values are in agreement with the literature (Angelo et al., 1995; Clouet, 2006) when h is larger than 10 nm and 6 nm (in case of multipole and isolated dipole configurations, respectively). In other words, when h is lower than these minimal distances, the dislocations are too close to be in elastic equilibrium.

The deviation angle φ of dipole has been also determined for different dipole heights h. The results are presented in **figure 3(c)** in the case of multipole configuration. When the calculations are performed with an EAM potential, φ is different from zero for dipole heights between 10 nm and 45 nm. In this range, the angle's values are between 22° and 25° and are in agreement with angle calculated from equation (4) using the elastic theory of dislocations (equal to 23° for multipole configuration). Calculations performed with the MEAM potential also present the deviation angle φ which tends to 25° but for a smaller range, between 5 nm and 20 nm. Finally, **figure 3(d)** presents the deviation angle results as a function of h for isolated dipole configuration. In this case, the values of φ are larger than 40° when h is between 7 nm and 25 nm for the calculations with an EAM potential. This interval is lower when the atomic calculations have been carried out with MEAM potential (the interval is between 3.6 nm and 20 nm).

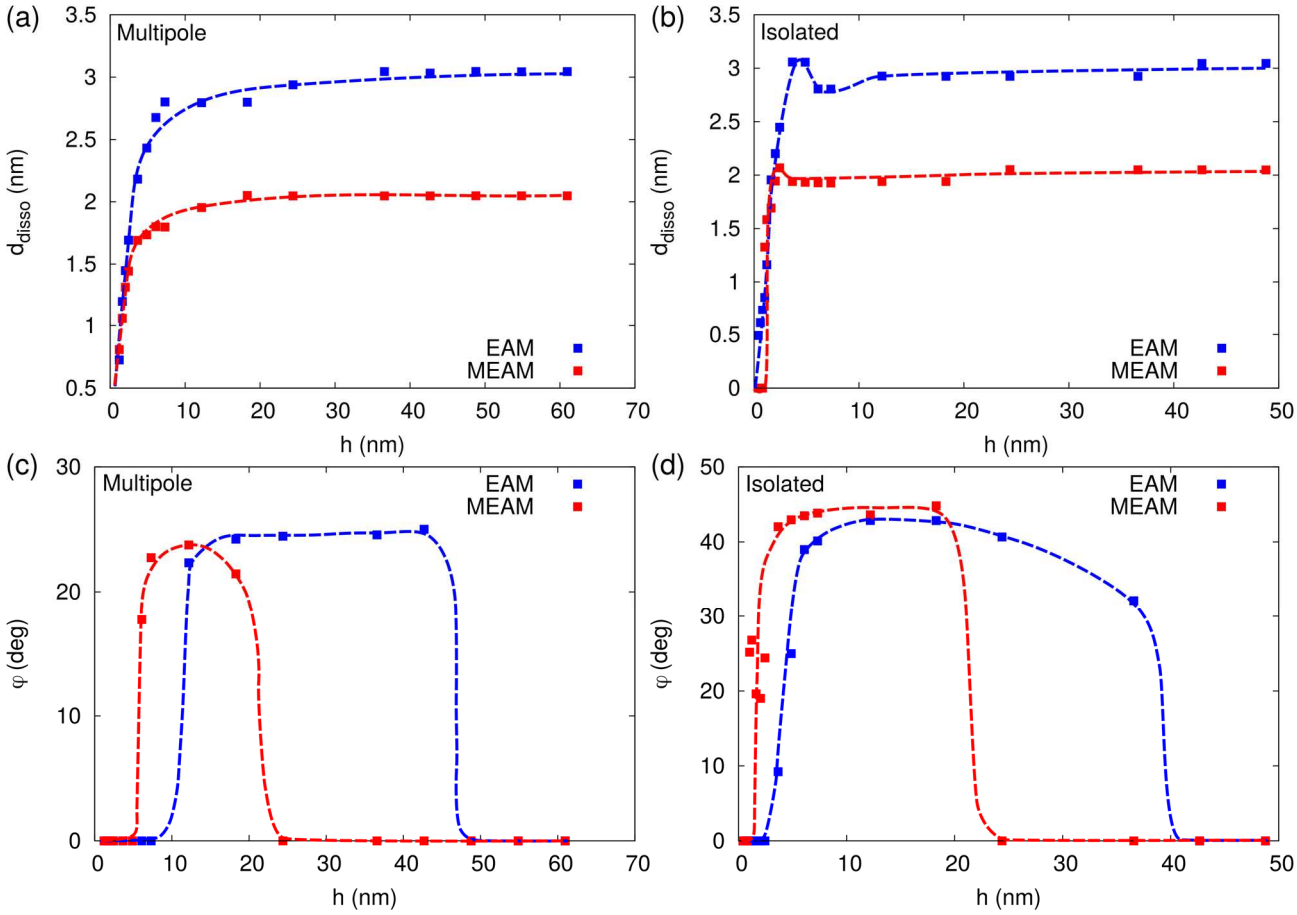

Figure 3: Dissociated distance d_{disso} of partial dislocations as a function of the dipole height in multipole (a) and in isolated dipole (b) configurations. Deviation angle φ of the dipole as a function of its height in multipole (c) and isolated dipole (d) configurations.

According to the isotropic elastic theory of dislocations, an isolated dipole of perfect edge dislocations without external forces is stable when the deviation angle is equal to 0° and 45° (Friedel, 1964; Hirth and Lothe, 1982). In the vicinity of $x = h$, a minor variation of φ has been noted when the dislocations are dissociated (Veyssière and Chiu, 2007). Similar values of φ have been obtained by atomic calculations at 0 K with both potentials. Moreover, according to the elastic theory of dislocations, we have noted that φ is equal to 23° and 67° when a dislocation interacts with its four nearest dislocation neighbours. With MD simulations, the deviation angle is approximately 23° when h is between 12 nm and 42 nm for EAM potential. When the calculations are performed with MEAM potential, φ= ~23° for when h is between 6 nm and 18 nm. The angle φ is equal to 0 when the height h of the dipole is beyond these intervals. It implies that dislocations are not too close or too far to interact as a dipole according to the elastic theory of dislocations.

Therefore, the deviation angle is a better parameter than the dissociation distance to evaluate the most suited potential for our study. A presentation of different multipole configurations with their corresponding deviation angle is shown in **table 1**. Three regions have been defined as a function of the dipole height h. The first region corresponds to dipoles too close to each other, inducing a deviation angle equal to 0. In this case, we obtain an aggregate, similar to a faulted dislocation dipole (*e.g.* h=1.2 nm in table 1) or an annihilation of dislocation, in agreement with the calculations made in the literature (Essmann and Mughrabi, 1979; Wang et al., 2013, 2008). A second region corresponds to dipole too far from each other, which also induces a deviation angle also equal to 0. The investigation of such configuration would be similar to study two isolated dislocations (*e.g.*

h=36.6 nm with MEAM potential in **table 1**). Finally, the third region corresponds to dipoles with their height in-between both regions (EAM: 10 nm<h<45 nm and MEAM: 5 nm<h<20 nm). In this case, the dislocations are stable and are in elastic equilibrium. Thus, the hydrogen atoms have been incorporated into these dipoles configurations. The same interpretation has been performed for isolated dipole dislocations when the dipole height is around 45°. In the case of calculations with EAM potential, the interval is 7 nm<h<25 nm whereas the obtained interval is 3.6 nm<h<20 nm for calculations performed with MEAM potential. Assuming the multipole configuration is similar to a Taylor lattice (equidistant dislocation dipoles), we obtain a dislocation density ρ equal to $1/(2h^2)$ (Cai and Nix, 2016). Hence, when h is between 10 nm and 45 nm, we get a dislocation density between 2.5×10^{14} m^{-2} and 50×10^{14} m^{-2}. These values are slightly larger than the density measured in the first part of the study ($\sim 3.00 \times 10^{14}$ m^{-2}). However, no elastic interaction between dislocation dipoles has been observed when h is larger than 45 nm. Therefore, we need to perform the atomic calculations in this interval, but the simulation cell containing a dipole height of 48.8 nm conduced to a dislocation densities in the range of the ones measured in the companion article

Although the EAM potential slightly overestimates the dissociation distance, we noted a larger interval of dipole height where the configuration is in elastic equilibrium compared to MEAM potential. Thus, the consequences of hydrogen and vacancies on the stability of edge dislocation dipoles have been evaluated exclusively with EAM potential in the interval of dipole height described previously.

Table 1: 2D views of relaxed simulation cells for different dipole heights in a multipole configurations with their corresponding deviation angle. For each image, the colour of each atom correspond to its potential energy.

	EAM potential		MEAM potential		
h (nm)	2D representation	φ	2D representation	φ	
1.2	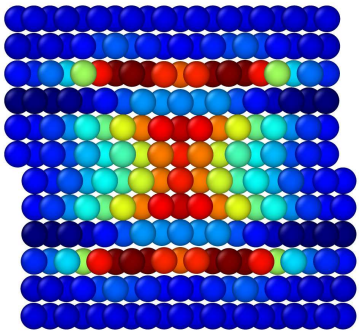	0°	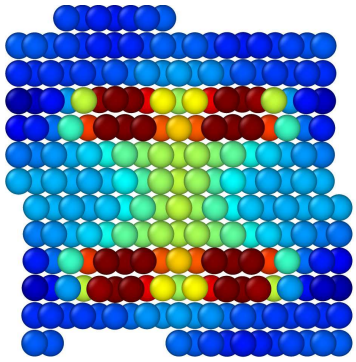	0°	E_{pot} > -4.35 eV
6.1	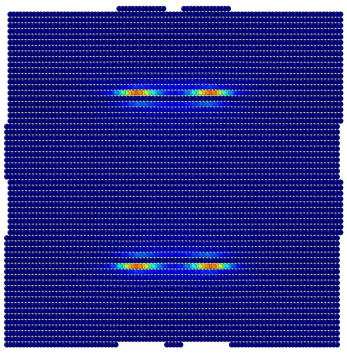	0°	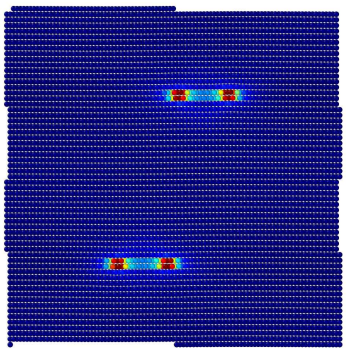	23°	
12.2	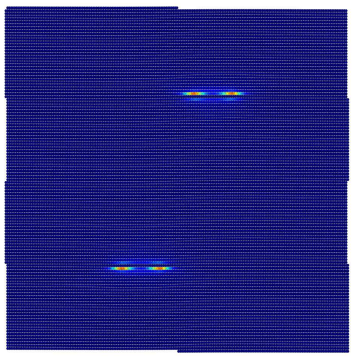	23°	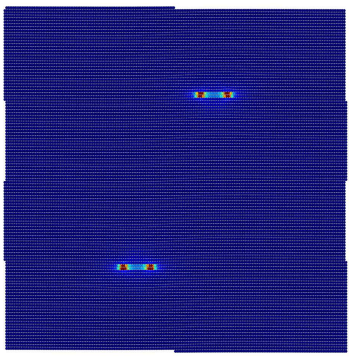	23°	
36.6	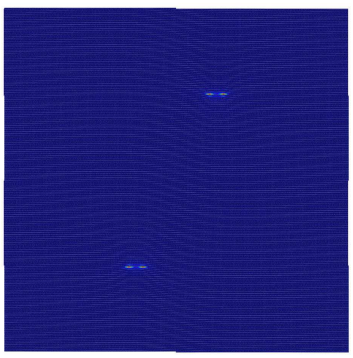	23°	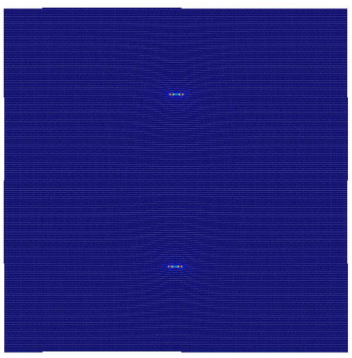	0°	E_{pot} < -4.45 eV

3.2 Evolution of the critical passing stress of dipole in the presence of hydrogen

Hydrogen atoms have been incorporated into the tensile zone (with P>10 GPa) of both dislocations of the dipole. However, it has been noted that this area is larger when the dipole height h is lower for both multipole and isolated dipole configurations. Therefore, a larger local hydrogen concentration is obtained when h is lower even if the same amount of hydrogen atoms is incorporated. **Table 2** presents the different local hydrogen concentrations, c_H^{400} and c_H^{800} correspond to concentrations when 400 and 800 hydrogen atoms are incorporated into the simulation cells (or when 200 or 400 hydrogen atoms incorporated in both Cottrell's atmosphere). Moreover, it has been also noted that this area is identical for a given dipole height h whether it is a multipole or isolated dipole configurations.

Table 2: Radius of the Cottrell's atmosphere R and the number of nickel atoms N_{Ni} in the Cottrell's atmosphere of the different simulations cells. c_H^{400} and c_H^{800} are the local hydrogen concentrations when 200 and 400 hydrogen atoms have been respectively incorporated in both Cottrell's atmosphere of the dislocation dipole for the different simulation.

			Local hydrogen concentration	
h (nm)	R (nm)	N_{Ni} (1.10^4 at.)	c_H^{400} (1.10^{-2} H/Ni)	c_H^{800} (1.10^{-2} H/Ni)
6.1	2.73	1.46	1.368	2.735
12.2	2.54	1.27	1.572	3.145
18.3	2.55	1.28	1.559	3.117
24.4	2.03	0.81	2.485	4.970
36.6	1.93	0.74	2.711	5.423
48.8	1.82	0.66	3.016	6.031

The MD calculations of nickel-hydrogen systems aim to evaluate the stability of edge dislocation dipoles in the presence of hydrogen. First, we have observed a reduction of the dissociation distance when the solute is incorporated in the Cottrell's atmosphere. **Figure 4** presents the observed decreases with the increase of hydrogen concentration. From the elastic theory of dislocations, we can assume the stacking fault energy is inversely proportional to the dissociation distance (Friedel, 1964; Hirth and Lothe, 1982; Hull and Bacon, 2011). Thus, an increase of the stacking fault energy is noted when the solute is introduced. This result is in agreement with previous calculations performed with empirical potentials (Tang and El-Awady, 2012; von Pezold et al., 2011). However, this observation is valid only for edge dislocation dipoles. For dissociated screw dislocations, hydrogen can be located in different area in the vicinity of the defect and can have an opposite effect on the stacking fault energy (Delafosse, 2012; Tang and El-Awady, 2012). Such behaviour is predicted with equations developed to describe the shielding effect of hydrogen in FCC metals (Chateau et al., 2002; Delafosse, 2012) and impacts the dislocation density in wall phase.

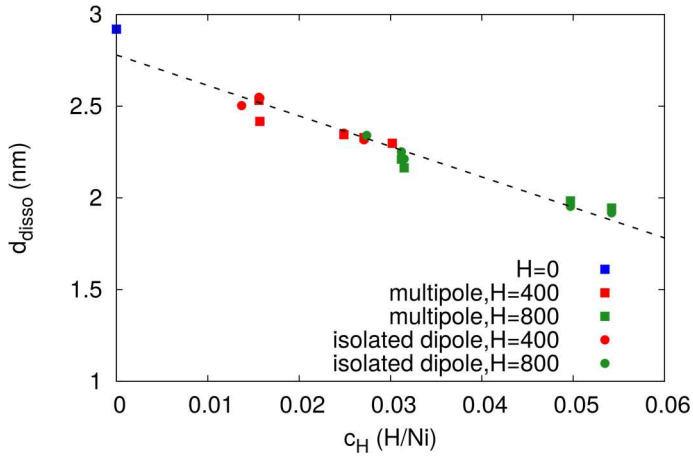

Figure 4: Dissociation distance as a function of the local hydrogen concentration in the vicinity of edge dislocation dipoles.

Then, the simulation cells have been relaxed at 100 K and the last energy minimisation has been performed at 0 K, before being sheared under a strain rate of 10^8 s^{-1} at 1 K (**figure 5(a)**). During the shearing of the simulation cell, edge dislocations move in their glide plane.

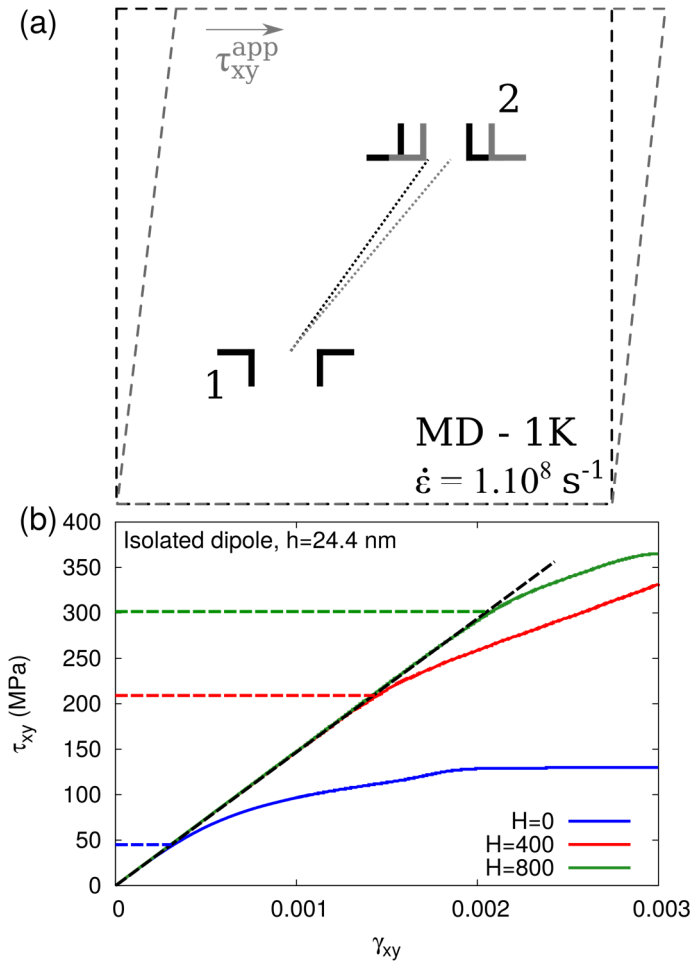

Figure 5: Sketch of the simulation cell containing a dipole configuration, sheared at 1 K with a strain rate of 1.10^8 s^{-1} (a). Corresponding stress-strain curves obtained when the dipole configuration has 0,

400 and 800 H atoms, respectively (b). The critical passing stress of dislocation dipoles are determined when the stress-strain curves lost its linear behaviour.

The resistance to this displacement due to dislocation/dislocation and dislocation/solute interactions leads mostly to a linear relationship between τ and γ. The end of this linearity defines a critical threshold for the breaking of dislocation dipoles, which can be assimilated to the critical passing stress τ_P. Hence, we can determine this critical stress from the MD simulations, by evaluating the end of the linear behaviour of the stress-strain curves. An example is given in **figure 5.(b)** (for an isolated dipole configuration with a dipole height of 24.4 nm) while the other curves are available in **supplementary materials 3**.

When hydrogen has been incorporated into the Cottrell's atmosphere of both edge dislocations, an increase of the critical passing stress has been noted. Hence, the evolution of the resulted critical stress has been represented as a function of the dipole height for pure nickel and nickel-hydrogen systems in **figure 6**. In addition, theoretical predictions by equations (4) and (2) have also been drawn in **figure 6(a)** and **figure 6(b)**, respectively for pure nickel. In the case of a solute-free multipole configuration, a slight difference is noted between the analytical results and the atomic-scale calculations. This difference should mainly be due to the hypothesis that dislocation/dislocation interactions are limited to its closest neighbouring dislocations (which are at a distance inferior or equal to $2h$).

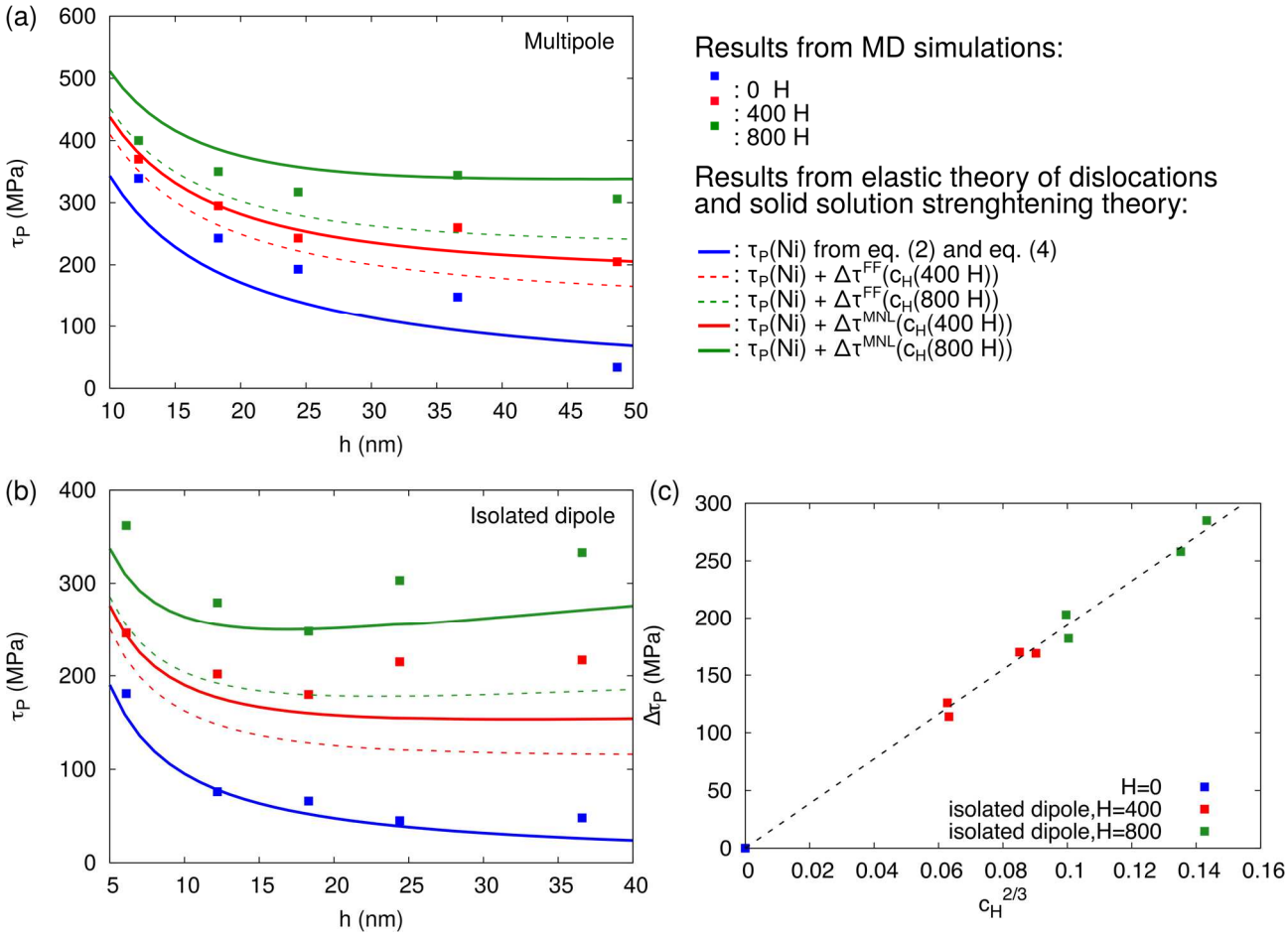

Figure 6: Critical passing stress τ_P as a function of the dipole height for different hydrogen concentrations in multipole (a) and isolated dipole (b) configurations (from models and MD simulations). The dashed lines represents the evolution of τ_P(Ni-H) determined with the Friedel-

Fleischer model (equation (6)). The lines represent the evolution of the critical passing stress calculated with the Mott-Nabarro-Labusch model (equation (7)). Critical stress τ_P as a function of the hydrogen concentration into the Cottrell's atmosphere for isolated dipole configuration (c).

The analytical form of the critical passing stress of Ni-H systems $\tau_P(\text{Ni-H})$ has also been drawn assuming:

$$\tau_P(\text{Ni-H}) = \tau_P(\text{Ni}) + \Delta\tau(c_H) \quad (8)$$

With $\Delta\tau(c_H)$ the hardening due to the solute, which has been described by models from Friedel-Fleischer and Mott-Nabarro-Labusch (presented with dashed line and line in **figure 6**, respectively). Finally, we assumed a maximum interaction force f_{max} about 1.4×10^{-10} N. This force is in the same order of the estimated 1×10^{-10} N, which corresponds to the maximum interaction force of an exclusively spherical distortion from impurities in materials (Haasen, 1979; Kubin, 1993). The curves obtained from the FF model seems to underestimate the impact of hydrogen while curves obtained with the MNL model gives critical stress in agreement with the atomic scale calculations. This result is consistent since the solute has been incorporated homogeneously into the Cottrell's atmosphere of dislocations and the value η_0 has always remained larger to 1 for all hydrogen concentrations. Finally, when the hardening obtained from MD simulations is represented as a function of $c_H^{2/3}$ for different dipole height (**figure 6(c)**), a linear behaviour has been noted. This observation confirms that hydrogen hardens τ_P according to the MNL model, hence the solute impacts the stability of edge dislocation dipoles in nickel according to the solid solution strengthening theory. However the results are in agreement with the analytical approach when the maximum interaction force f_{max} is fixed at 1.4×10^{-10} N. Therefore, in the first part of this discussion, we have to verify this value.

3.3 Stability of edge dislocation dipole in the presence of vacancies.

Then, MD simulations have been performed with vacancies, in addition to hydrogen, since it is well known that hydrogen and fatigue induce the formation of vacancies (Carr and McLellan, 2004; Fukai, 2005; Man et al., 2009; Metsue et al., 2014; Saada and Veyssière, 2002). Therefore, vacancies and hydrogen may occupy the same regions in the vicinity of edge dislocation dipoles. In **supplementary material 1**, we noted that formed vacancies in the Cottrell's atmosphere are not stable without hydrogen. Consequently, we introduced vacancies in the configuration containing hydrogen. Since these point defects have been formed before the thermal relaxation at 100K, hydrogen atoms can segregate near vacancies during this thermal relaxation (an example of Cottrell's atmosphere containing hydrogen and vacancies has been presented in **figure 7(a)**). Therefore, we have first evaluated the minimal distance between 100 hydrogen atoms and 100 vacancies presented in **figure 7(b)**.

When hydrogen is trapped into vacancies, the distance between them is about 0.176 nm (Metsue et al., 2016). However, larger minimal distance between vacancy and hydrogen for the MD simulations has been noted and is about 0.497 nm. This difference is observed because the diffusion coefficient of vacancy is very low compared to the diffusion coefficient of hydrogen (Metsue et al., 2016). The relaxation at 100 K allows the solute to move from tetrahedral to octahedral interstitial sites but the temperature is not large enough to allow the diffusion of vacancy. However, hydrogen atoms are still in the vicinity of vacancies, therefore, we have supposed that the formation of this defect with the incorporation of hydrogen into the Cottrell's atmosphere is enough to describe the

interaction hydrogen-vacancy-dislocation. Additionally, this configuration seems more realistic in fatigue, where we have multiple sources of production of vacancies.

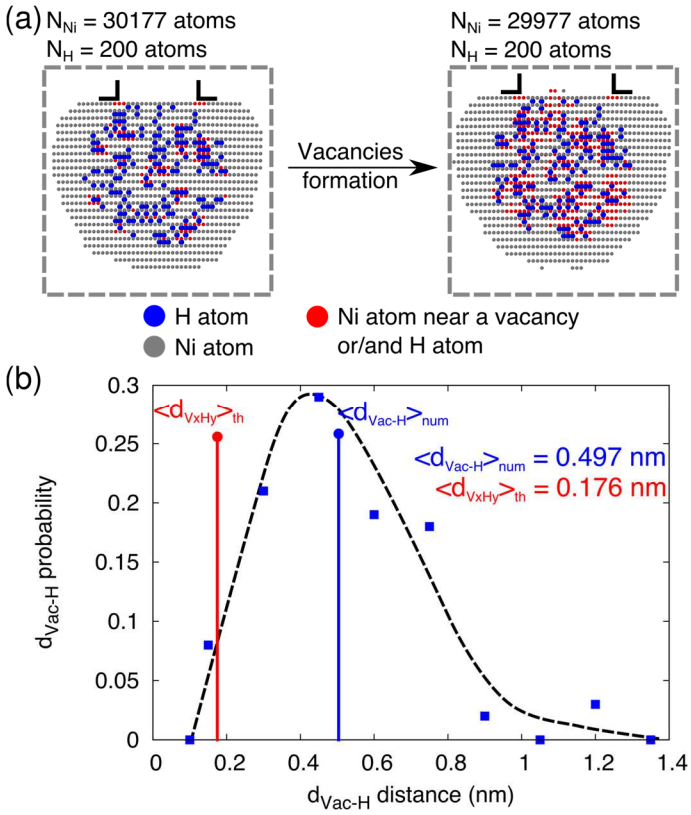

Figure 7: Cottrell's atmosphere containing hydrogen around a dislocation with nickel atoms in grey. The red colour indicates the nickel atoms has a hydrogen atom or a vacancy around it (the coordination number of the atoms is different than 12). The atoms in blue represent hydrogen atoms (a). Minimal vacancy-hydrogen distance distribution in Cottrell atmosphere around dislocation (b).

When the simulation cells are relaxed at 0K after the thermal relaxation in the presence of vacancies, a decrease of the dissociation distance has still been noted but it was less important than vacancy-free Cottrell's atmosphere. Such results imply that vacancies induced by hydrogen incorporation and cyclic loadings attenuate the effect of hydrogen on the increase of the stacking fault energy.

Then, simulation cells containing vacancies have been sheared under the same conditions as previously described (at 1K under a strain rate of 10^8 s^{-1}). The critical stress τ_P of simulation cells with vacancies has also been evaluated from the obtained shear stress-shear strain curves. They have been presented as a function of the height h in **figure 8(a)** and **figure 8(b)** for multipole and isolated dipole configurations, respectively. Previously, we noted an increase of τ_P following the MNL model when hydrogen was incorporated into the Cottrell's atmosphere of dislocations for both configurations. When vacancies are formed (in addition to the incorporation of hydrogen), attenuation of this increase is noted for each simulation.

Finally, we have also sheared atomic simulation cells containing isotropic sphere of vacancies about 0.8 nm in each Cottrell's atmosphere of the different simulation cells containing hydrogen atoms. The results are also presented in **figure 8(a)** for multipole and **figure 8(b)** with isolated dipole

configurations. We noted that when the vacancies are regrouped, the attenuation is larger for all dipole heights for both configurations.

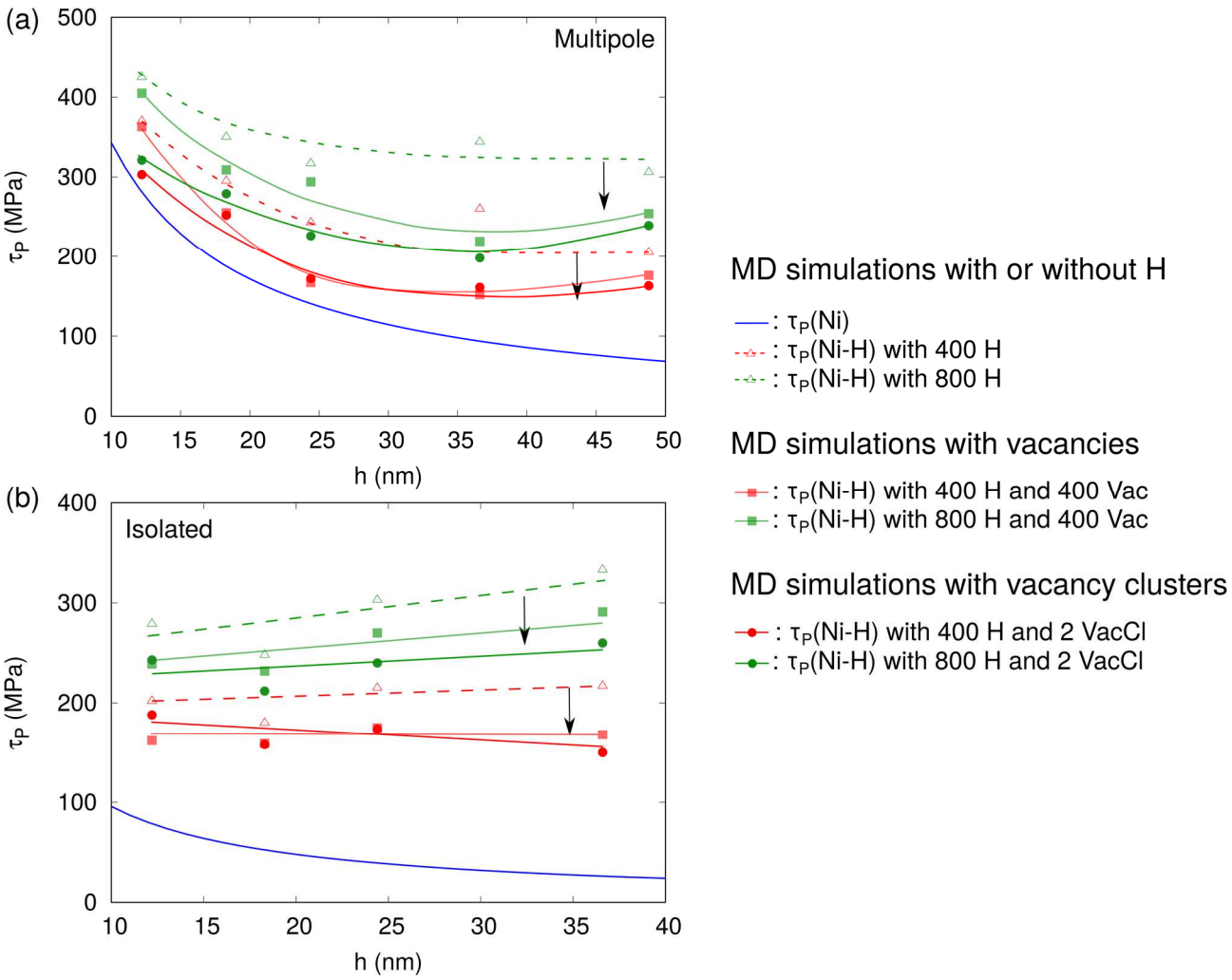

Figure 8: Critical passing stress τ_P as a function of the dipole height for different hydrogen concentration in multipole (a) and isolated dipole (b) configurations with and without vacancies and vacancy clusters.

4. Discussion

The stability of edge dislocation dipoles of nickel single crystal in the presence of hydrogen and vacancies has been investigated in order to understand the evolution of the back stress and hydrogen hardening of wall phases noted in previous work (Hachet et al., 2019). The simulation can be representative of the behaviour of edge dislocation dipoles containing in the wall phase of the dislocation structures induced by fatigue. However, we only describe an established fatigue structure and we questioned its stability when an external stress is applied. These conditions were not representative to the dynamic of dislocation pattern under fatigue loadings; therefore, it was necessary to use models from elastic theory of dislocations. We have obtained similar results with both methods (critical passing stress for different dipoles height and concentration of hydrogen). Specific attention has been realised to the understanding of hydrogen-vacancy-dislocation interactions. Calculations on the stability of dipolar configurations in pure nickel have been firstly performed at 0 K using two empirical interatomic potentials. Although calculations performed with MEAM potential have given dissociation distances closers to ones reported in the literature (Clouet, 2006), dipoles seemed to be

in elastic equilibrium for a wider range of dipole height when the calculations are performed with EAM potential. Therefore, the stability of dipoles with hydrogen and vacancies has been conducted with the potential of Angelo *et al.* (Angelo et al., 1995).

When hydrogen has been incorporated and the thermal relaxation performed, a decrease of the stacking fault ribbon has first been noted. This effect can correspond to an increase of the stacking fault energy obtained with empirical calculations (Tang and El-Awady, 2012; von Pezold et al., 2011) and predicted with equations based on the shielding consequences of hydrogen (Chateau et al., 2002; Delafosse, 2012) in FCC metals. Such behaviour is consistent with the noted increase of the dislocation density in wall phase measured for cyclically pre-strained nickel-hydrogen systems at different hardening stages, which are presented in part I of the study.

Moreover, in order to evaluate the stability of such configurations, we have evaluated the critical passing stress τ_P when the dipole has been sheared at 1 K with and without hydrogen and vacancies. In parallel, an analytical approach has been developed using the elastic theory of dislocations and the solid solution strengthening theory of these defects. MD simulations show that hydrogen hardens the metal when it is incorporated in the Cottrell atmosphere of dislocation. In the first part of the discussion, we purpose to verify the chosen value of f_{max} (supposed at 1.4×10^{-10} N).

Furthermore, we noted that when vacancies are formed in the Cottrell's atmosphere containing hydrogen, an attenuation of the effect of hydrogen is observed for all dipole configurations. In order to understand the evolution of the back stress reported in the first part this work (Hachet et al., 2019), it is mandatory to evaluate the concentration of vacancies formed by the incorporation of hydrogen when it is pre-charged electrochemically and chemically. The second part of this discussion is focused on these measurements in addition to the correlation between the calculations performed at the atomic scale with the results obtained at macro-scale.

4.1 Validation of the MNL model used to describe the hardening of edge dislocation dipoles due to hydrogen incorporation

We purpose to verify the chosen value of maximum interaction force by determining the $\Delta\tau_P(C_H)$ from the segregation energy e_{seg} of hydrogen atoms of a sheared simulation cell containing dislocation dipoles (here, we choose an isolated dipole configuration with h=18.3 nm). As a reminder, when 200 hydrogen atoms are incorporated into each Cottrell's atmosphere of this configuration, we have noted $\Delta\tau_P(C_H)$ equal to 127 MPa with equation (7).

In the followings, we have assumed that the hydrogen segregation of each atoms e_{seg} is the difference of energy equal to (Hull and Bacon, 2011):

$$e_{seg} = e_{tot}(x) - e_{tot}(x = 0) \tag{9}$$

With $e_{tot}(x)$ the internal energy of the hydrogen atoms when the dislocation moves from x nm along its glide plane and $e_{tot}(x = 0)$ the energy of each solute when the dislocation is at its initial position before the shearing of the simulation cell. For the sake of clarity, we have assumed that each hydrogen atom has been situated in the centre of the Cottrell's atmosphere, then we have analytically expressed the hydrogen segregation energy of the solutes calculated with MD simulations as a function of the position of the dislocation in its glide plane *via* (Hull and Bacon, 2011):

$$E_{seg} = \sum e_{seg} = -A \frac{r_0}{(x^2 + r_0^2)^2} \times n_H \quad (10)$$

With n_H the number of hydrogen atoms, r_0 the distance between the centre of the Cottrell's atmosphere and the middle of the stacking fault of the dissociated dislocation along the Y axis and A a coefficient equal to (Hull and Bacon, 2011):

$$A = G \times b \times \Omega_A \times |\delta| \quad (11)$$

G and Ω_A correspond to the isotropic shear modulus and the atomic volume of nickel, respectively. Ω_A is equal to 10.93×10^{-3} nm³/At and the shear modulus has been calculated from the Voigt-Reuss-Hill average of the elastic constants determined by *ab initio* calculations in previous study (Hachet et al., 2018). Finally, the value $|\delta|$ corresponds to a distortion parameter due to the incorporation of the solute, equal to (Kubin, 1993):

$$|\delta| = \frac{1}{a} \frac{da}{dc_H} \quad (12)$$

From the relative expansion of Ni-matrix from the incorporation of hydrogen presented in the supplementary materials of previous study (Hachet et al., 2018), we obtain $|\delta| = 6.7\%$. Hence, the segregation energy of hydrogen atoms has been determined as a function of the position of the dislocation from atomic calculations and with equation (10). The result has been presented in **figure 9(a)**. The analytic expression follows the evolution determined by calculation with MD simulations. Therefore, the projected interaction force F_{seg} between the solutes and the dislocation in the x direction has been calculated by deriving equation (10), *i.e.*:

$$F_{seg} = \frac{dE_{seg}}{dx} = \frac{2Ar_0}{(x^2 + r^0)^2} \times n_H \quad (13)$$

Figure 9(b) presents the evolution of this force as a function of the position x. The force has a maximum ($F_{max} = 2.86 \times 10^{-12} N$) when the distance between the centre of the Cottrell atmosphere and the middle of the dissociated dislocation along the X axis is equal to 1.87 nm. Thus the maximum stress τ_{seg} needed to break the elastic equilibrium between the solutes and the dislocation can be deduced using the following expression:

$$\tau_{seg} = \frac{F_{seg}}{b \times l_z} \quad (14)$$

With l_z the length of the dislocation line along the Z axis (equal to $16 \times a\sqrt{3/2}$, for this configuration). Hence, we deduced a maximum segregation stress τ_{seg} equal to 166 MPa. This stress is close to the 127 MPa determined using the MNL model and validates the analytical approach used in this work. It also confirms that hydrogen hardens dislocations following the solid solution strengthening theory.

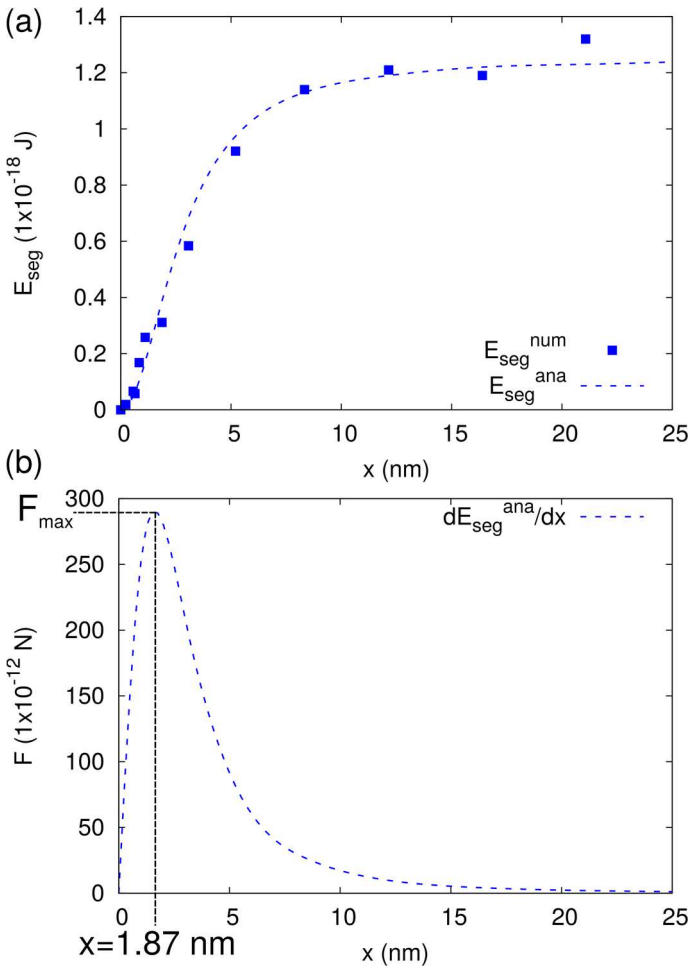

Figure 9: Evolution of the segregation energy of hydrogen atoms with the dislocation position along its slip plane from MD simulations and equation (10) (a). Interaction force between the Cottrell atmosphere and the dislocation deduced from equation (13) (b).

Finally, when vacancies are formed in addition to the incorporation of the solute, we noted an attenuation of this hardening. **Figure 10** presents an increase of the critical stress τ_P as a function of $c_H^{2/3}$ with and without vacancies homogeneously distributed or regrouped as an isotropic spherical cluster. We noted the behaviour of τ_P is still linear in the presence of vacancy. In other words, the critical stress still follows an additive forms depending on the solute concentration with a correction factor, which depends on the elastic distortion of the defect. This result is complementary to EAM calculations performed by Tehranchi *et al.* where the authors have observed that vacancies formed homogeneously in the vicinity of edge dislocations in nickel single crystal increased the required stress to move the dislocation (Tehranchi et al., 2017). Furthermore, a larger attenuation is noted for all hydrogen concentration when these defects have been regrouped as a vacancy cluster. Therefore, vacancies clusters have a larger impact on the stability of edge dislocation dipoles than homogeneously distributed vacancies in the presence of hydrogen.

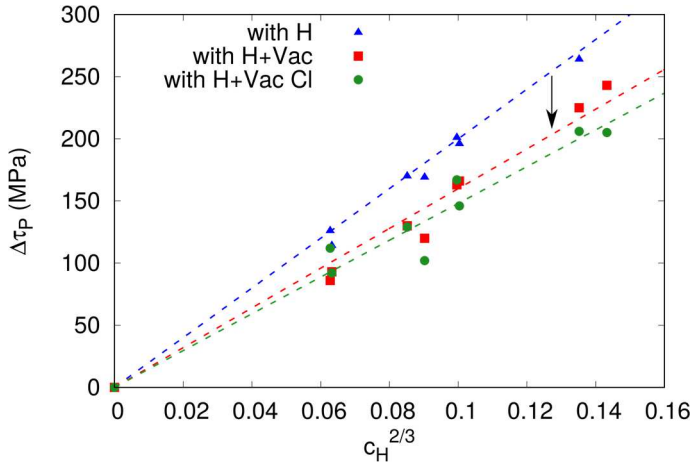

Figure 10: Increase of critical stress τ_P as a function of the hydrogen concentration into the Cottrell atmosphere for isolated dipole configuration.

Since vacancies, besides hydrogen atoms, have an impact on the stability of edge dislocation dipoles, they should impact the wall phase induced by fatigue. Therefore, the concentration of vacancies needs to be quantified when the solute has been pre-charged electrochemically and chemically in nickel single crystal in order to explain the noted evolution of the back stress presented in the first part of this study (Hachet et al., 2019).

4.2 Evolution of the back stress: determination of the vacancy concentration for the different hydrogen charging mode

From atomic calculations, we noted that hydrogen hardens edge dislocation dipoles, but vacancies and vacancy clusters induced by hydrogen incorporation attenuate the impact of the solute. In order to verify the consequences of this result at the macroscale, we have determined the vacancy concentration of electrochemically and chemically pre-charged (charging methods described in part I of the study) nickel single crystal. The vacancy concentration has been determined through differential scanning calorimetry (DSC) measurements. The samples have been pre-charged under the same conditions as detailed in the previous article with several hydrogen charging time. To determine the concentration of vacancies C_{Vac}, we first evaluated stored energy E_{Vac}^{st} from the heat flow curves, then C_{Vac} has been using the following equation (Oudriss et al., 2012; Setman et al., 2008):

$$C_{Vac} = \frac{E_{Vac}^{st}}{e_{Vac}} \times \frac{N_A}{M_{\mathrm{Ni}}} \tag{15}$$

With e_{Vac} the formation energy of vacancies in nickel single crystal, determined at 1.49 eV at 300 K with *ab initio* calculations (Metsue et al., 2014a), N_A the Avogadro number, M_{Ni} the molar mass of the host metal. More details of the experimental procedure and the analysis of the DSC curves to determine the vacancy concentration C_{Vac} are given in **supplementary material 4**. The measured vacancy concentration is presented in **figure 11(a)** when the solute is incorporated electrochemically at 298K and chemically at 323K. Although the hydrogen concentration is larger when the solute is incorporated chemically, a lower vacancy concentration is noted. Such evolution can be explained by the temperature of the solution (equal to 323 K), which is large enough to observe vacancy annihilation, but also it can be explained by the hydrogen charging time. For a given amount of hydrogen incorporated into the sample, the hydrogen charging time is lower when it is incorporated

chemically than when it is incorporated electrochemically. Therefore, fewer vacancies have been formed when the solute is incorporated chemically.

Hence, the behaviour of cyclically strained nickel single crystal can be described from these DSC measurements, the composite model of the dislocation structures induced by fatigue described in part I of this study and the MD calculations performed on the stability of edge dislocation dipoles. In the first part of the study, a softening has been observed for hardening stages II_0 and III_0 when hydrogen is pre-charged in nickel single crystal, in addition to a minor hardening noted in the stage III. Then, the saturated stress has been decomposed into internal stresses corresponding to the short and long-range interactions of dislocations called effective τ_{eff} and back τ_X stresses, respectively. Assuming the dislocation structures induced by fatigue is similar to a composite model composed of channel and wall phases, we noted that hydrogen reduces the effective stress for all plastic strain amplitudes and has a more complicated impact on the back stress. Since the plastic flow is easier in channel phase than in wall phase, we suggest that the effective stress corresponds to the stress induced by channel phase τ_c (Feaugas, 2003; Mughrabi, 1988, 1983). Using the composite model of dislocation structures, the back stress can be written as follows:

$$\tau_X = f_w \times (\tau_w - \tau_c) \tag{16}$$

With f_w, the fraction of wall structures, evaluated in part I of the study. Then assuming a Taylor's hardening of each dislocation phase, the stresses induced by channel τ_c and wall τ_w phases can be written:

$$\tau_c = \alpha_c \mu(C_{Vac}) b \sqrt{\rho_c(C_H)} \tag{17}$$

$$\tau_w = \alpha_w \mu(C_{Vac}) b \sqrt{\rho_w(C_H)} + \Delta\tau_w(C_H, C_{Vac}) \tag{18}$$

With b the Burgers vector, α_i the hardening coefficient which depends on the hardening stage, but has a minor variation when hydrogen is incorporated. The shear modulus $\mu(C_{Vac})$ depends on the elastic constants of the nickel-hydrogen systems. In previous work, we have observed that hydrogen has a minor effect on such constants but defects induced by the incorporation of the solute have a more important impact (Hachet et al., 2018). In channel phase, the solute reduces τ_c which also reduces dislocation densities of this phase ρ_c. However, when the solute has been chemically and electrochemically incorporated two different behaviours on the back stress τ_X have been highlighted. Therefore, from the measurements of ρ_w in part I of the study, the DSC measurements and these calculations, we suggest the stress induced by wall phase still follows a Taylor hardening. However, it also follows a hardening according to solid solution theory, which depends on the concentration of hydrogen and vacancies.

Thus, when hydrogen is incorporated chemically, a relatively large hydrogen concentration (~8.10^{-4} H/Ni) with a relatively low vacancy concentration (~3.10^{-4} Vac/Ni) is introduced. In this case, hydrogen in Cottrell's atmosphere hardens the edge dislocation dipoles and increase the back stress for all plastic strain amplitudes according to solid solution theory (mechanism 1 in **figure 11(b)**). However, when the solute is incorporated electrochemically, the vacancy concentration is approximately identical to the concentration of hydrogen (~4.10^{-4} Vac/Ni and ~4.10^{-4} H/Ni, respectively). The vacancies due to hydrogen incorporation, which are present in Cottrell atmosphere, attenuate the hardening due to hydrogen and reduces the back stress for all plastic strain amplitudes (mechanism 2 in **figure 11(b)**).

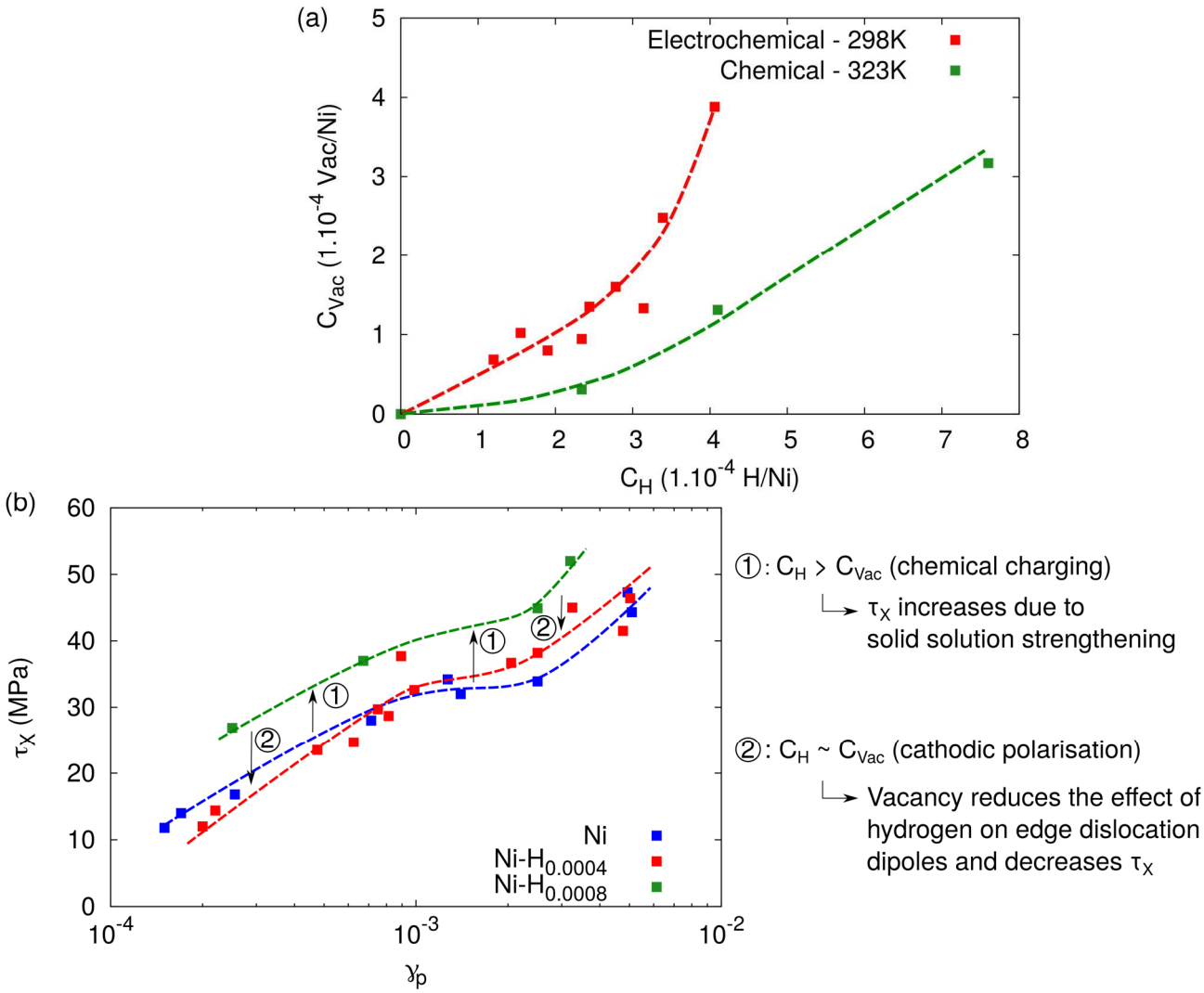

Figure 11: Vacancy concentration as a function of the hydrogen concentration when the solute is introduced electrochemically and chemically (a). Back stress τ_X of Ni-H systems with several hydrogen concentrations as a function of the plastic strain amplitude (b).

5. Conclusions

In the second part of this study, we have conducted atomic calculations on edge dislocation dipoles in nickel single crystal in order to evaluate their stability in the presence of hydrogen, vacancies and vacancy clusters. The results presented in this work are:

- In case of hydrogen and vacancies free simulation cells, we noted that calculations with MEAM potential presents dissociated dislocations more in agreement with the literature (the dissociation distance is closer the ones calculated from the stacking fault energy).
- The dislocation-dislocation interaction is in agreement with the elastic theory of dislocation for a wider range of dipole height in case of calculations performed with EAM potential.
- The stability of edge dislocation dipoles in nickel with hydrogen and vacancies has been evaluated by determining the critical passing stress of the system from numerical and analytical approaches.
- Hydrogen in Cottrell's atmosphere hardens the dislocation dipoles following a Mott-Nabarro-Labush model. Vacancies and vacancy clusters attenuate this result.

- The attenuation of vacancies is more important when they are regrouped as clusters than when they are homogeneously regrouped.
- The complex behaviour of the back stress noted in the first part of this study has been affiliated with the stress induced by walls structure. When hydrogen is incorporated chemically, the large concentration of hydrogen and the low concentration of vacancies induced a hardening following the solid solution strengthening theory. In contrast, when hydrogen is incorporated electrochemically, the concentration of hydrogen is approximately equal to the concentration of vacancy. These defects attenuate the consequences of the solute on edge dislocation dipoles.

From this study composed of two articles, we managed to characterise the effect of hydrogen on the cyclically strained nickel single crystal oriented for multi-slips at different length scales. We noted that hydrogen effect implicates antagonist processes (hardening and softening) at different scales. The softening process is associated to a decrease of the dislocations densities in the channel phase, in addition to the formation of vacancies clusters which affects the elastic properties. The hardening process occurs mainly in wall phase with the segregation of hydrogen in elastic field of edge dislocations dipoles.

Kinetic effects of hydrogen should be also considered, the first results of jump frequency has been previously performed (Metsue et al., 2018) and will be investigated in the future. Moreover, previous numerical study has highlighted the formation of nanohydride around edge dislocations which induces a strong and short-range shielding effect (von Pezold et al., 2011). Such effect should also be investigated in contrast with the consequences vacancy formation around dislocations in our future studies

Acknowledgments

The authors would like to acknowledge the funding from French Research National Agency (ANR) through the CRACKHINIT project (Contract ANR-17-CE08-0023-01).

References

Angelo, J.E., Moody, N.R., Baskes, I., 1995. Trapping of hydrogen to lattice defects in nickel.
Antonopoulos, J.G., Brown, L.M., Winter, A.T., 1976. Vacancy dipoles in fatigued copper. Philos. Mag. 34, 549–563. https://doi.org/10.1080/14786437608223793
Argon, A.S., 1996. Mechanical properties of single-phase crystalline media: Deformation at low temperatures, in: Physical Metallurgy. Elsevier, pp. 1877–1955.
Beachem, C.D., 1972. A new model for hydrogen-assisted cracking (hydrogen “embrittlement”). Metall. Mater. Trans. B 3, 441–455. https://doi.org/10.1007/BF02642048
Bhatia, M.A., Groh, S., Solanki, K.N., 2014. Atomic-scale investigation of point defects and hydrogen-solute atmospheres on the edge dislocation mobility in alpha iron. J. Appl. Phys. 116, 064302. https://doi.org/10.1063/1.4892630
Birnbaum, H.K., Sofronis, P., 1994. Hydrogen-enhanced localized plasticity—a mechanism for hydrogen-related fracture. Mater. Sci. Eng. A 176, 191–202. https://doi.org/10.1016/0921-5093(94)90975-X
Bonneville, J., Escaig, B., 1979. Cross-slipping process and the stress-orientation dependence in pure copper. Acta Metall. 27, 1477–1486. https://doi.org/10.1016/0001-6160(79)90170-6
Cahn, J.W., Haasen, P., 1996. Physical Metallurgy, 4th ed. North-Holland.
Cai, W., Nix, W.D., 2016. Imperfections in Crystalline Solids, MRS-Cambridge Materials. Cambridge University Press.

Carr, N.Z., McLellan, R.B., 2004. The thermodynamic and kinetic behavior of metal–vacancy–hydrogen systems. Acta Mater. 52, 3273–3293. https://doi.org/10.1016/j.actamat.2004.03.024
Castelluccio, G.M., Geller, C.B., McDowell, D.L., 2018. A rationale for modeling hydrogen effects on plastic deformation across scales in FCC metals. Int. J. Plast. 111, 72–84. https://doi.org/10.1016/j.ijplas.2018.07.009
Chang, J., Cai, W., Bulatov, V.V., Yip, S., 2002. Molecular dynamics simulations of motion of edge and screw dislocations in a metal. Comput. Mater. Sci. 23, 111–115. https://doi.org/10.1016/S0927-0256(01)00221-X
Chateau, J.P., Delafosse, D., Magnin, T., 2002. Numerical simulations of hydrogen–dislocation interactions in fcc stainless steels. Part I: hydrogen–dislocation interactions in bulk crystals. Acta Mater. 16.
Clouet, E., 2006. The vacancy-edge dislocation interaction in fcc metals: A comparison between atomic simulations and elasticity theory. Acta Mater. 54, 3543–3552.
Connétable, D., Wang, Y., Tanguy, D., 2014. Segregation of hydrogen to defects in nickel using first-principles calculations: The case of self-interstitials and cavities. J. Alloys Compd. 614, 211–220. https://doi.org/10.1016/j.jallcom.2014.05.094
Cottrell, A.H., 1953. Dislocations and plastic flow in crystals, International Series of Monographs on Physics. Oxford University Press.
Delafosse, D., 2012. Hydrogen effects on the plasticity of face centred cubic (fcc) crystals, in: Gaseous Hydrogen Embrittlement of Materials in Energy Technologies. Elsevier, pp. 247–285. https://doi.org/10.1533/9780857095374.2.247
Delafosse, D., Magnin, T., 2001. Hydrogen induced plasticity in stress corrosion cracking of engineering systems. Eng. Fract. Mech. 68, 693–729. https://doi.org/10.1016/S0013-7944(00)00121-1
Erel, C., Po, G., Crosby, T., Ghoniem, N., 2017. Generation and interaction mechanisms of prismatic dislocation loops in FCC metals. Comput. Mater. Sci. 140, 32–46. https://doi.org/10.1016/j.commatsci.2017.07.043
Escaig, B., 1968. Sur le glissement dévié des dislocations dans la structure cubique à faces centrées. J. Phys. 29, 225–239. https://doi.org/10.1051/jphys:01968002902-3022500
Essmann, U., Mughrabi, H., 1979. Annihilation of dislocations during tensile and cyclic deformation and limits of dislocation densities. Philos. Mag. A 40, 731–756. https://doi.org/10.1080/01418617908234871
Feaugas, X., 2003. Tensile and cyclic hardening: Back and effective stresses concepts and their applications. Recent Res. Mater. Sci. 4, 35–64.
Feaugas, X., Delafosse, D., 2019. Chapter 9: Hydrogen and Crystal Defects Interactions: Effects on Plasticity and Fracture, in: Mechanics - Microstructure - Corrosion Coupling. Elsevier Publisher, pp. 199–222.
Fleischer, R.L., 1963. Substitutional solution hardening. Acta Metall. 11.
Fourie, J.T., Murphy, R.J., 1962. Elongated dislocation loops and the stress-strain properties of copper single crystals. Philos. Mag. 7, 1617–1631. https://doi.org/10.1080/14786436208213699
Friedel, J., 1964. Dislocations. Pergamon Press.
Fukai, Y., 2005. The metal-hydrogen system: basic bulk properties, 2. ed, Materials Science. Springer, Berlin.
Girardin, G., Delafosse, D., 2004. Measurement of the saturated dislocation pinning force in hydrogenated nickel and nickel base alloys. Scr. Mater. 51, 1177–1181. https://doi.org/10.1016/j.scriptamat.2004.07.012
Gu, Y., El-Awady, J.A., 2018. Quantifying the effect of hydrogen on dislocation dynamics: A three-dimensional discrete dislocation dynamics framework. J. Mech. Phys. Solids 112, 491–507. https://doi.org/10.1016/j.jmps.2018.01.006
Haasen, P., 1979. Dislocations in SOlids, in: Dislocations in Solids. North-Holland, pp. 155–189.

Hachet, G., 2018. Multi-scale investigation of the consequences of hydrogen on the mechanical response of cyclically strained nickel single crystal. Université de La Rochelle.
Hachet, G., Metsue, A., Oudriss, A., Feaugas, X., 2018. Influence of hydrogen on the elastic properties of nickel single crystal: A numerical and experimental investigation. Acta Mater. 148, 280–288. https://doi.org/10.1016/j.actamat.2018.01.056
Hachet, G., Oudriss, A., Barnoush, A., Milet, R., Wan, D., Metsue, A., Feaugas, X., 2019. Effect of hydrogen on the mechanical response of <001> oriented nickel single crystal. Part I: Experimental investigation International Journal of Plasticity.
Hallil, A., Metsue, A., Oudriss, A., Bouhattate, J., Feaugas, X., 2018. Segregation energy of the hydrogen at Ni Σ3 grain boundaries: some implications of the atomic volume and the interstitial self-stress. J. Mater. Sci. 53, 5356–5363. https://doi.org/10.1007/s10853-017-1941-5
Harada, S., Yokota, S., Ishii, Y., Shizuku, Y., Kanazawa, M., Fukai, Y., 2005. A relation between the vacancy concentration and hydrogen concentration in the Ni–H, Co–H and Pd–H systems. J. Alloys Compd. 404–406, 247–251. https://doi.org/10.1016/j.jallcom.2005.02.077
Hirth, J.P., Lothe, P., 1982. Theory of dislocations, 2nd ed. Wiley.
Hull, D., Bacon, D.J., 2011. Introduction to dislocations, fifth. ed. Elsevier Science.
Kirchheim, R., 1981. Interaction of hydrogen with dislocations in palladium--I. Activity and diffusivity and their phenomenological interpretation. Acta Metall. 29, 835–843.
Ko, W.-S., Shim, J.-H., Lee, B.-J., 2011. Atomistic modeling of the Al–H and Ni–H systems. J. Mater. Res. 26, 1552–1560. https://doi.org/10.1557/jmr.2011.95
Kroupa, F., 1966. Dislocation dipoles and dislocation loops. J. Phys. Colloq. 27, C3-154-C3-167. https://doi.org/10.1051/jphyscol:1966320
Kubin, L.P., 1993. Dislocation partterming, in: Mughrabi, H. (Ed.), Plastic Deformation and Fracture of Materials. VCH.
Labusch, R., 1970. A Statistical Theory of Solid Solution Hardening. Phys. Status Solidi B 41, 659–669. https://doi.org/10.1002/pssb.19700410221
Laird, C., 1996. Fatigue, in: Physical Metallurgy. Elsevier, pp. 2293–2397.
Lee, B.-J., Shim, J.-H., Baskes, M.I., 2003. Semiempirical atomic potentials for the fcc metals Cu, Ag, Au, Ni, Pd, Pt, Al, and Pb based on first and second nearest-neighbor modified embedded atom method. Phys. Rev. B 68. https://doi.org/10.1103/PhysRevB.68.144112
Li, P., Li, S.X., Wang, Z.G., Zhang, Z.F., 2011. Fundamental factors on formation mechanism of dislocation arrangements in cyclically deformed fcc single crystals. Prog. Mater. Sci. 56, 328–377. https://doi.org/10.1016/j.pmatsci.2010.12.001
Li, S., Li, Y., Lo, Y.-C., Neeraj, T., Srinivasan, R., Ding, X., Sun, J., Qi, L., Gumbsch, P., Li, J., 2015. The interaction of dislocations and hydrogen-vacancy complexes and its importance for deformation-induced proto nano-voids formation in α-Fe. Int. J. Plast. 74, 175–191. https://doi.org/10.1016/j.ijplas.2015.05.017
Lynch, S.P., 2019. Discussion of some recent literature on hydrogen-embrittlement mechanisms: addressing common misunderstandings. Corros. Rev. Accepted.
Magnin, T., Bosch, C., Wolski, K., Delafosse, D., 2001. Cyclic plastic deformation behaviour of Ni single crystals oriented for single slip as a function of hydrogen content. Mater. Sci. Eng. A 314, 7–11. https://doi.org/10.1016/S0921-5093(00)01920-1
Man, J., Obrtlík, K., Polák, J., 2009. Extrusions and intrusions in fatigued metals. Part 1. State of the art and history†. Philos. Mag. 89, 1295–1336. https://doi.org/10.1080/14786430902917616
Metsue, A., Oudriss, A., Feaugas, X., 2018. Trapping/detrapping kinetic rates of hydrogen around a vacancy in nickel and some consequences on the hydrogen-vacancy clusters thermodynamic equilibrium. Comput. Mater. Sci. 151, 144–152. https://doi.org/10.1016/j.commatsci.2018.05.013
Metsue, A., Oudriss, A., Feaugas, X., 2016. Hydrogen solubility and vacancy concentration in nickel single crystals at thermal equilibrium: New insights from statistical mechanics and ab initio calculations. J. Alloys Compd. 656, 555–567. https://doi.org/10.1016/j.jallcom.2015.09.252

Metsue, A., Oudriss, A., Feaugas, X., 2014. Displacement field induced by a vacancy in nickel and some implications for the solubility of hydrogen. Philos. Mag. 94, 3978–3991. https://doi.org/10.1080/14786435.2014.975769
Mughrabi, H., 1988. Dislocation clustering and long-range internal stresses in monotonically and cyclically deformed metal crystals. Rev. Phys. Appliquée 23, 367–379. https://doi.org/10.1051/rphysap:01988002304036700
Mughrabi, H., 1987. The long-range internal stress field in the dislocation wall structure of persistent slip bands. Phys. Status Solidi A 104, 107–120. https://doi.org/10.1002/pssa.2211040108
Mughrabi, H., 1983. Dislocation wall and cell structures and long-range internal stresses in deformed metal crystals. Acta Metall. 31, 1367–1379.
Nagumo, M., 2016. Fundamentals of hydrogen embrittlement. Springer Singapore.
Nazarov, R., Hickel, T., Neugebauer, J., 2014. *Ab initio* study of H-vacancy interactions in fcc metals: Implications for the formation of superabundant vacancies. Phys. Rev. B 89. https://doi.org/10.1103/PhysRevB.89.144108
Oudriss, A., Creus, J., Bouhattate, J., Conforto, E., Berziou, C., Savall, C., Feaugas, X., 2012. Grain size and grain-boundary effects on diffusion and trapping of hydrogen in pure nickel. Acta Mater. 60, 6814–6828. https://doi.org/10.1016/j.actamat.2012.09.004
Patinet, S., Proville, L., 2008. Depinning transition for a screw dislocation in a model solid solution. Phys. Rev. B 78. https://doi.org/10.1103/PhysRevB.78.104109
Plimpton, S., 1995. Fast Parallel Algorithms for Short–Range Molecular Dynamics 42.
Polak, J., 1969. Electrical resistivity of cyclically deformed copper 9.
Price, P.B., 1961. On dislocation loops formed in zinc crystals during low temperature pyramidal glide. Philos. Mag. 6, 449–451. https://doi.org/10.1080/14786436108235899
Rao, S.I., Dimiduk, D.M., El-Awady, J.A., Parthasarathy, T.A., Uchic, M.D., Woodward, C., 2010. Activated states for cross-slip at screw dislocation intersections in face-centered cubic nickel and copper via atomistic simulation. Acta Mater. 58, 5547–5557. https://doi.org/10.1016/j.actamat.2010.06.005
Rao, S.I., Dimiduk, D.M., Parthasarathy, T.A., El-Awady, J., Woodward, C., Uchic, M.D., 2011. Calculations of intersection cross-slip activation energies in fcc metals using nudged elastic band method. Acta Mater. 59, 7135–7144. https://doi.org/10.1016/j.actamat.2011.08.029
Robertson, I.M., Birnbaum, H.K., Sofronis, P., 2009. Chapter 91: Hydrogen effects on plasticity, in: Dislocations in Plasticity. Elsevier Amsterdam.
Robertson, I.M., Sofronis, P., Nagao, A., Martin, M.L., Wang, S., Gross, D.W., Nygren, K.E., 2015. Hydrogen Embrittlement Understood. Metall. Mater. Trans. B 46, 1085–1103. https://doi.org/10.1007/s11663-015-0325-y
Saada, G., 1991. Cross-slip and work hardening of f.c.c. crystals. Mater. Sci. Eng. A 137, 177–183. https://doi.org/10.1016/0921-5093(91)90333-I
Saada, G., 1960. Sur le durcissement dû à la recombinaison des dislocations. Acta Metall. 8, 841–847. https://doi.org/10.1016/0001-6160(60)90150-4
Saada, G., Veyssière, P., 2002. Chapter 61: Work hardening of face centred cubic crystals. Dislocations intersection and cross slip, in: Dislocations in Solids. Elsevier, pp. 413–458. https://doi.org/10.1016/S1572-4859(02)80012-2
Sato, K., Yoshiie, T., Ishizaki, T., Xu, Q., 2004. Anistropic motion of point defects near edge dislocations. J. Nucl. Mater. 329–333, 929–932.
Segall, R.L., Partridge, P.G., Hirsch, P.B., 1961. The dislocation distribution in face-centred cubic metals after fatigue. Philos. Mag. 6, 1493–1513. https://doi.org/10.1080/14786436108243392
Sofronis, P., Birnbaum, H.K., 1995. Mechanics of the hydrogen-dislocation-impurity interactions- I. Increasing shear modulus. J. Mech. Phys. Solids 43, 42.

Stukowski, A., 2010. Visualization and analysis of atomistic simulation data with OVITO–the Open Visualization Tool. Model. Simul. Mater. Sci. Eng. 18, 015012. https://doi.org/10.1088/0965-0393/18/1/015012
Tang, Y., El-Awady, J.A., 2012. Atomistic simulations of the interactions of hydrogen with dislocations in fcc metals. Phys. Rev. B 86. https://doi.org/10.1103/PhysRevB.86.174102
Tehranchi, A., Curtin, W.A., 2017. Atomistic study of hydrogen embrittlement of grain boundaries in nickel: I. Fracture. J. Mech. Phys. Solids 101, 150–165. https://doi.org/10.1016/j.jmps.2017.01.020
Tehranchi, A., Yin, B., Curtin, W.A., 2017. Softening and hardening of yield stress by hydrogen–solute interactions. Philos. Mag. 97, 400–418. https://doi.org/10.1080/14786435.2016.1263402
Tetelman, A.S., 1962. The pinching-off of dislocation dipoles by glide. Philos. Mag. 7, 1801–1816. https://doi.org/10.1080/14786436208213847
Tichy, G., Essmann, U., 1989. Modelling of edge dislocation dipoles in face-centred-cubic lattices. Philos. Mag. B 60, 503–512. https://doi.org/10.1080/13642818908205923
Tippelt, B., Breitschneider, J., Hähner, P., 1997. The Dislocation Microstructure of Cyclically Deformed Nickel Single Crystals at Different Temperatures. Phys. Status Solidi A 163, 11–26. https://doi.org/10.1002/1521-396X(199709)163:1<11::AID-PSSA11>3.0.CO;2-X
Varvenne, C., Leyson, G.P.M., Ghazisaeidi, M., Curtin, W.A., 2017. Solute strengthening in random alloys. Acta Mater. 124, 660–683. https://doi.org/10.1016/j.actamat.2016.09.046
Veyssière, P., Chiu, Y.-L., 2007. Equilibrium and passing properties of dislocation dipoles. Philos. Mag. 87, 3351–3372. https://doi.org/10.1080/14786430601021678
von Pezold, J., Lymperakis, L., Neugebeauer, J., 2011. Hydrogen-enhanced local plasticity at dilute bulk H concentrations: The role of H–H interactions and the formation of local hydrides. Acta Mater. 59, 2969–2980. https://doi.org/10.1016/j.actamat.2011.01.037
Wang, H., Xu, D., Yang, R., Veyssière, P., 2008. The transformation of edge dislocation dipoles in aluminium. Acta Mater. 56, 4608–4620. https://doi.org/10.1016/j.actamat.2008.05.019
Wang, H., Xu, D.S., Rodney, D., Veyssière, P., Yang, R., 2013. Atomistic investigation of the annihilation of non-screw dislocation dipoles in Al, Cu, Ni and γ -TiAl. Model. Simul. Mater. Sci. Eng. 21, 025002. https://doi.org/10.1088/0965-0393/21/2/025002
Wen, M., Fukuyama, S., Yokogawa, K., 2007. Cross-slip process in fcc nickel with hydrogen in a stacking fault: An atomistic study using the embedded-atom method. Phys. Rev. B 75. https://doi.org/10.1103/PhysRevB.75.144110
Xu, X., Wen, M., Hu, Z., Fukuyama, S., Yokogawa, K., 2002. Atomistic process on hydrogen embrittlement of a single crystal of nickel by the embedded atom method. Comput. Mater. Sci. 23, 131–138. https://doi.org/10.1016/S0927-0256(01)00217-8
Zhao, K., He, J., Mayer, A.E., Zhang, Z., 2018. Effect of hydrogen on the collective behavior of dislocations in the case of nanoindentation. Acta Mater. 148, 18–27. https://doi.org/10.1016/j.actamat.2018.01.053
Zhou, X., Ouyang, B., Curtin, W.A., Song, J., 2016. Atomistic investigation of the influence of hydrogen on dislocation nucleation during nanoindentation in Ni and Pd. Acta Mater. 116, 364–369. https://doi.org/10.1016/j.actamat.2016.06.061
Zhou, X.W., Dingreville, R., Karnesky, R.A., 2018. Molecular dynamics studies of irradiation effects on hydrogen isotope diffusion through nickel crystals and grain boundaries. Phys. Chem. Chem. Phys. 20, 520–534. https://doi.org/10.1039/C7CP06086F
Zhu, Y., Li, Z., Huang, M., Fan, H., 2017. Study on interactions of an edge dislocation with vacancy-H complex by atomistic modelling. Int. J. Plast. 92, 31–44. https://doi.org/10.1016/j.ijplas.2017.03.003